13 Energy Transfer

Fluorescence resonance energy transfer (FRET) has become widely used in all applications of fluorescence, including medical diagnostics, DNA analysis, and optical imaging. The widespread use of FRET is due to the favorable distances for energy transfer, which are typically the size of a protein or the thickness of a membrane. Additionally, the extent of FRET is readily predictable from the spectral properties of the fluorophores. If the spectral properties of the fluorophores allow FRET, it will occur and will not be significantly affected by the biomolecules in the sample. These favorable properties allow for the design of experiments based on the known sizes and structural features of the sample.

FRET is an electrodynamic phenomenon that can be explained using classical physics. FRET occurs between a donor (D) molecule in the excited state and an acceptor (A) molecule in the ground state. The donor molecules typically emit at shorter wavelengths that overlap with the absorption spectrum of the acceptor. Energy transfer occurs without the appearance of a photon and is the result of long-range dipole–dipole interactions between the donor and acceptor. The term resonance energy transfer (RET) is preferred because the process does not involve the appearance of a photon. The rate of energy transfer depends upon the extent of spectral overlap of the emission spectrum of the donor with the absorption spectrum of the acceptor, the quantum yield of the donor, the relative orientation of the donor and acceptor transition dipoles, and the distance between the donor and acceptor molecules. The distance dependence of RET allows measurement of the distances between donors and acceptors.

The most common application of RET is to measure the distances between two sites on a macromolecule. Typically a protein is covalently labeled with a donor and an acceptor (Figure 13.1). In studies of protein structure the donor is often a tryptophan residue. However, extrinsic donors are often used because of the opportunity to position the donor in a desired location and to select the D–A pairs that are most suitable for a particular application. If there is a single donor and acceptor, and if the D–A distance does not change during the excited-state lifetime, then the D–A distance can be determined from the efficiency of energy transfer. The transfer efficiency can be determined by steady-state measurements of the extent of donor quenching due to the acceptor.

RET is also used in studies in which the actual D–A distance is not being measured. Typical experiments of this type include DNA hybridization or any bioaffinity reactions. If the sample contains two types of macromolecules that are individually labeled with donor or acceptor, association of the molecules can usually be observed using RET. The observation of RET is sufficient to measure the extent of binding, even without calculation of the D–A distance. At present, steady-state measurements are often used to measure binding interactions. Distances are usually obtained from time-resolved measurements.

Resonance energy transfer is also used to study macromolecular systems when there is more than a single acceptor molecule near a donor molecule. This situation often occurs for larger assemblies of macromolecules, or when using membranes where the acceptor is a freely diffusing lipid analogue. Even with a single D–A pair, there can be more than a single D–A distance, such as for an unfolded protein. The extent of energy transfer can also be influenced by the presence of donor-to-acceptor diffusion during the donor lifetime. Although information can be obtained from the steady-state data, such systems are usually studied using time-resolved measurements. These more advanced applications of RET are presented in Chapters 14 and 15.

13.1. CHARACTERISTICS OF RESONANCE ENERGY TRANSFER

The distance at which RET is 50% efficient is called the Förster distance,[1] which is typically in the range of 20 to 60

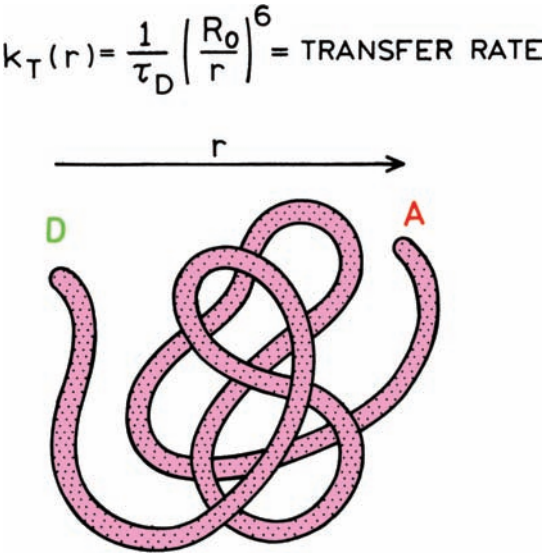

Figure 13.1. Fluorescence resonance energy transfer (FRET) for a protein with a single donor (D) and acceptor (A).

Å. The rate of energy transfer from a donor to an acceptor $k_T(r)$ is given by

$$k_T(r) = \frac{1}{\tau_D}\left(\frac{R_0}{r}\right)^6 \qquad (13.1)$$

where τ_D is the decay time of the donor in the absence of acceptor, R_0 is the Förster distance, and r is the donor-to-acceptor distance. Hence, the rate of transfer is equal to the decay rate of the donor ($1/\tau_D$) when the D-to-A distance (r) is equal to the Förster distance (R_0), and the transfer efficiency is 50%. At this distance ($r = R_0$) the donor emission would be decreased to half its intensity in the absence of acceptors. The rate of RET depends strongly on distance, and is proportional to r^{-6} (eq. 13.1).

Förster distances ranging from 20 to 90 Å are convenient for studies of biological macromolecules. These distances are comparable to the size of biomolecules and/or the distance between sites on multi-subunit proteins. Any condition that affects the D–A distance will affect the transfer rate, allowing the change in distance to be quantified. In this type of application, one uses the extent of energy transfer between a fixed donor and acceptor to calculate the D–A distance, and thus obtain structural information about the macromolecule (Figure 13.1). Such distance measurements have resulted in the description of RET as a "spectroscopic ruler."[2,3] For instance, energy transfer can be used to measure the distance from a tryptophan residue to a ligand binding site when the ligand serves as the acceptor.

In the case of multi-domain proteins, RET has been used to measure conformational changes that move the domains closer or further apart. Energy transfer can also be used to measure the distance between a site on a protein and a membrane surface, association between protein subunits, and lateral association of membrane-bound proteins. In the case of macromolecular association reactions one relies less on determination of a precise D–A distance, and more on the simple fact that energy transfer occurs whenever the donors and acceptors are in close proximity comparable to the Förster distance.

The use of energy transfer as a proximity indicator illustrates an important characteristic of energy transfer. Energy transfer can be reliably assumed to occur whenever the donors and acceptors are within the characteristic Förster distance, and whenever suitable spectral overlap occurs. The value of R_0 can be reliably predicted from the spectral properties of the donors and acceptors. Energy transfer is a through-space interaction that is mostly independent of the intervening solvent and/or macromolecule. In principle, the orientation of the donors and acceptors can prevent energy transfer between a closely spaced D–A pair, but such a result is rare and possibly nonexistent in biomolecules. Hence one can assume that RET will occur if the spectral properties are suitable and the D–A distance is comparable to R_0. A wide variety of biochemical interactions result in changes in distance and are thus measurable using RET.

It is important to remember that resonance energy transfer is a process that does not involve emission and reabsorption of photons. The theory of energy transfer is based on the concept of a fluorophore as an oscillating dipole, which can exchange energy with another dipole with a similar resonance frequency.[4] Hence RET is similar to the behavior of coupled oscillators, like two swings on a common supporting beam. In contrast, radiative energy transfer is due to emission and reabsorption of photons, and is thus due to inner filter effects. Radiative transfer depends upon non-molecular optical properties of the sample, such as the size of the sample container, the path length, the optical densities of the sample at the excitation and emission wavelengths, and the geometric arrangement of the excitation and emission light paths. In contrast to these trivial factors, non-radiative energy transfer contains a wealth of structural information concerning the donor–acceptor pair.

Resonance energy transfer contains molecular information that is different from that revealed by solvent relaxation, excited-state reactions, fluorescence quenching, or fluorescence anisotropy. These other fluorescence phenomena depend on interactions of the fluorophore with other molecules in the surrounding solvent shell. These nearby interactions are less important for energy transfer, except for their effects on the spectral properties of the donor and acceptor. Non-radiative energy transfer is effective over much longer distances, and the intervening solvent or macromolecule has little effect on the efficiency of energy transfer, which depends primarily on the D–A distance. In this chapter we will describe the basic theory of non-radiative energy transfer and the applications of RET to biochemical systems. The biochemical applications of RET have been the subject of several reviews (additional references on RET and protein folding are listed near the end of this chapter). More complex formalisms are needed to describe other commonly encountered situations, such as distance distributions (Chapter 14) and the presence of multiple acceptors (Chapter 15).

13.2. THEORY OF ENERGY TRANSFER FOR A DONOR–ACCEPTOR PAIR

The theory for resonance energy transfer is moderately complex, and similar equations have been derived from classical and quantum mechanical considerations. We will describe only the final equations. Readers interested in the physical basis of RET are referred to the excellent review by Clegg.[4] RET is best understood by considering a single donor and acceptor separated by a distance (r). The rate of transfer for a donor and acceptor separated by a distance r is given by

$$k_T(r) = \frac{Q_D \kappa^2}{\tau_D r^6}\left(\frac{9000(\ln 10)}{128\pi^5 N n^4}\right)\int_0^\infty F_D(\lambda)\,\varepsilon_A(\lambda)\,\lambda^4 d\lambda \qquad (13.2)$$

where Q_D is the quantum yield of the donor in the absence of acceptor, n is the refractive index of the medium, N is Avogadro's number, r is the distance between the donor and acceptor, and τ_D is the lifetime of the donor in the absence of acceptor. The refractive index (n) is typically assumed to be 1.4 for biomolecules in aqueous solution. $F_D(\lambda)$ is the corrected fluorescence intensity of the donor in the wavelength range λ to $\lambda + \Delta\lambda$ with the total intensity (area under the curve) normalized to unity. $\varepsilon_A(\lambda)$ is the extinction coefficient of the acceptor at λ, which is typically in units of M^{-1} cm^{-1}. The term κ^2 is a factor describing the relative orientation in space of the transition dipoles of the donor and acceptor. κ^2 is usually assumed to be equal to 2/3, which is appropriate for dynamic random averaging of the donor and acceptor (Section 13.2.1, below). In eq. 13.2 the transfer rate is written as a function of r, $k_T(r)$, to emphasize its dependence on distance.

The overlap integral ($J(\lambda)$) expresses the degree of spectral overlap between the donor emission and the acceptor absorption:

$$J(\lambda) = \int_0^\infty F_D(\lambda)\varepsilon_A(\lambda)\lambda^4 d\lambda = \frac{\int_0^\infty F_D(\lambda)\varepsilon_A(\lambda)\lambda^4 d\lambda}{\int_0^\infty F_D(\lambda)\,d\lambda} \qquad (13.3)$$

$F_D(\lambda)$ is dimensionless. If $\varepsilon_A(\lambda)$ is expressed in units of M^{-1} cm^{-1} and λ is in nanometers, then $J(\lambda)$ is in units of M^{-1} cm^{-1} nm^4. If λ is in centimeters then $J(\lambda)$ is in units of M^{-1} cm^3. In calculating $J(\lambda)$ one should use the corrected emission spectrum with its area normalized to unity (eq. 13.3, middle), or normalize the calculated value of $J(\lambda)$ by the area (eq. 13.3, right). The overlap integral has been defined in several ways, each with different units. In our experience we find it is easy to get confused, so we recommend the units of nm or cm for the wavelength, and units of M^{-1} cm^{-1} for the extinction coefficient.

In designing a biochemical experiment it is usually easier to think about distances than transfer rates. For this reason eq. 13.2 is written in terms of the Förster distance R_0. At this distance, half the donor molecules decay by energy transfer and half decay by the usual radiative and non-radiative rates. From eqs. 13.1 and 13.2 with $k_T(r) = \tau_D^{-1}$ one obtains

$$R_0^6 = \frac{9000(\ln 10)\kappa^2 Q_D}{128\pi^5 N n^4}\int_0^\infty F_D(\lambda)\,\varepsilon_A(\lambda)\,\lambda^4 d\lambda \qquad (13.4)$$

This expression allows the Förster distance to be calculated from the spectral properties of the donor and the acceptor and the donor quantum yield. While eq. 13.4 looks complex, many of the terms are simple physical constants. It is convenient to have simpler expressions for R_0 in terms of the experimentally known values, which is accomplished by combining the constant terms in equation 13.4. If the

wavelength is expressed in nm then $F_D(\lambda)$ is in units of M^{-1} cm^{-1} $(nm)^4$, and the Förster distance in Å is given by

$$R_0 = 0.211(\kappa^2 n^{-4} Q_D J(\lambda))^{1/6} \text{ (in Å)} \quad (13.5)$$

$$R_0^6 = 8.79 \times 10^{-5}(\kappa^2 n^{-4} Q_D J(\lambda)) \text{ (in Å}^6) \quad (13.6)$$

If the wavelength is expressed in cm and $J(\lambda)$ is in units of M^{-1} cm^3, the Förster distance is given by

$$R_0^6 = 8.79 \times 10^{-25}(\kappa^2 n^{-4} Q_D J(\lambda)) \text{ (in cm}^6) \quad (13.7)$$

$$R_0 = 9.78 \times 10^{3}(\kappa^2 n^{-4} Q_D J(\lambda))^{1/6} \text{ (in Å)} \quad (13.8)$$

$$R_0^6 = 8.79 \times 10^{23}(\kappa^2 n^{-4} Q_D J(\lambda)) \text{ (in Å}^6) \quad (13.9)$$

It is important to recognize that the Förster distances are usually reported for an assumed value of κ^2, typically $\kappa^2 = 2/3$. Once the value of R_0 is known the rate of energy transfer can be easily calculated using

$$k_T(r) = \frac{1}{\tau_D}\left(\frac{R_0}{r}\right)^6 \quad (13.10)$$

If the transfer rate is much faster than the decay rate, then energy transfer will be efficient. If the transfer rate is slower than the decay rate, then little transfer will occur during the excited-state lifetime, and RET will be inefficient.

The efficiency of energy transfer (E) is the fraction of photons absorbed by the donor which are transferred to the acceptor. This fraction is given by

$$E = \frac{k_T(r)}{\tau_D^{-1} + k_T(r)} \quad (13.11)$$

which is the ratio of the transfer rate to the total decay rate of the donor in the presence of acceptor. Recalling that $k_T(r) = \tau_D^{-1}(R_0/r)^6$, one can easily rearrange eq. 13.11 to yield

$$E = \frac{R_0^6}{R_0^6 + r^6} \quad (13.12)$$

This equation shows that the transfer efficiency is strongly dependent on distance when the D–A distance is near R_0 (Figure 13.2). The efficiency quickly increases to 1.0 as the D–A distance decreases below R_0. For instance, if $r = 0.1R_0$ one can readily calculate that the transfer efficiency is 0.999999, indicating that the donor emission would not be observable. Conversely, the transfer efficiency quickly decreases to zero if r is greater than R_0. Because E depends so strongly on distance, measurements of the distance (r) are only reliable when r is within a factor of 2 of R_0. If r is twice the Förster distance ($r = 2R_0$) then the transfer efficiency is 1.54%, and if $r = 0.5R_0$ then the efficiency is 98.5%. It is not practical to use RET to measure distances outside the range of $r = 0.5R_0$ to $r = 2R_0$.

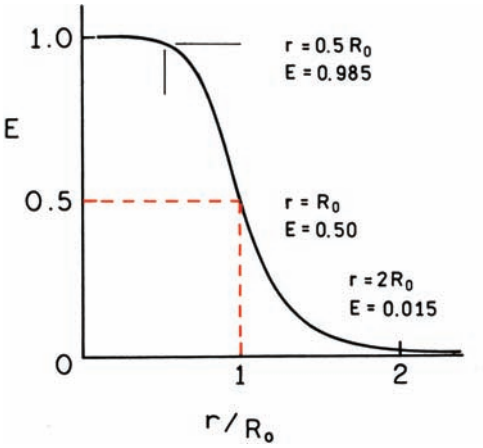

Figure 13.2. Dependence of the energy transfer efficiency (E) on distance. R_0 is the Förster distance.

The transfer efficiency is typically measured using the relative fluorescence intensity of the donor, in the absence (F_D) and presence (F_{DA}) of acceptor:

$$E = 1 - \frac{F_{DA}}{F_D} \quad (13.13)$$

The transfer efficiency can also be calculated from the lifetimes under these respective conditions (τ_{DA} and τ_D):

$$E = 1 - \frac{\tau_{DA}}{\tau_D} \quad (13.14)$$

It is important to remember the assumptions involved in using these equations. Equations 13.13 and 13.14 are only applicable to donor-acceptor pairs that are separated by a fixed distance, a situation frequently encountered for labeled proteins. However, a single fixed donor–acceptor distance is not found for a mixture of donors and acceptors in solution, nor for donors and acceptors dispersed random-

ly in membranes. More complex expressions are required in these cases, and such expressions are generally derived by averaging the transfer rate over the assumed spatial distribution of donor–acceptor pairs.[5–7]

The use of lifetimes in eq. 13.14 has been a source of confusion. In eq. 13.14 we have assumed that the decay of the donor is a single exponential in the absence (τ_D) and presence (τ_{DA}) of acceptor. Single-exponential decays are rare in biomolecules. If the intensity decays are multi-exponential then it is important to use an average decay time which is proportional to the steady-state intensity. These averages are given by the sum of the $\alpha_i\tau_i$ products. The decay rate in the presence of acceptor will only remain a single exponential if there is a single D–A distance. If the donor decay is a single exponential, the presence of acceptors at more than one distance can result in more complex decays (Chapter 14).

In order to calculate the D–A distance it is necessary to know R_0, which in turn depends upon κ^2, n, Q_D, and $J(\lambda)$. These values must be known to calculate the distance. The refractive index is generally known from the solvent composition or is estimated for the macromolecule. The refractive index is often assumed to be near that of water (n = 1.33) or small organic molecules (n = 1.39). The quantum yield of the donor (Q_D) is determined by comparison with standard fluorophores. Since Q_D is used as the sixth root in the calculation of R_0, small errors in Q_D do not have a large effect on R_0. For instance, if the quantum yield is increased by a factor of 2 the $R0$ value is still correct to within ±12%. The overlap integral must be evaluated for each D–A pair. The greater the overlap of the emission spectrum of the donor with the absorption spectrum of the acceptor, the higher the value of R_0. Acceptors with larger extinction coefficients result in larger R_0 values. In the equations presented above it was assumed that the lifetime of the donor was not altered by binding of the acceptor, other than by the rate of energy transfer. For labeled macromolecules this may not always be the case. Allosteric interactions between the donor and acceptor sites could alter the donor lifetime by enhancement of other decay processes, or by protection from these processes. Under these circumstances more complex analysis of the apparent transfer efficiency is required, typically a comparison of the apparent efficiency by donor quenching and enhanced acceptor emission.

The dependence of R_0 on spectral overlap is illustrated in Figure 13.3 for transfer from structural isomers of dansyl-labeled phosphatidylethanolamine (DPE) to the eosin-labeled lipid (EPE). Each of the dansyl derivatives of DPE displays a different emission spectrum.[5] As the spectra of the DPE isomers shift to longer wavelengths the overlap with the absorption spectrum of EPE increases and the R_0 values increase (Table 13.1). One notices that R_0 is not very dependent upon $J(\lambda)$. For instance, for two of the D–A pairs a 120-fold change in the overlap integral results in a 2.2-

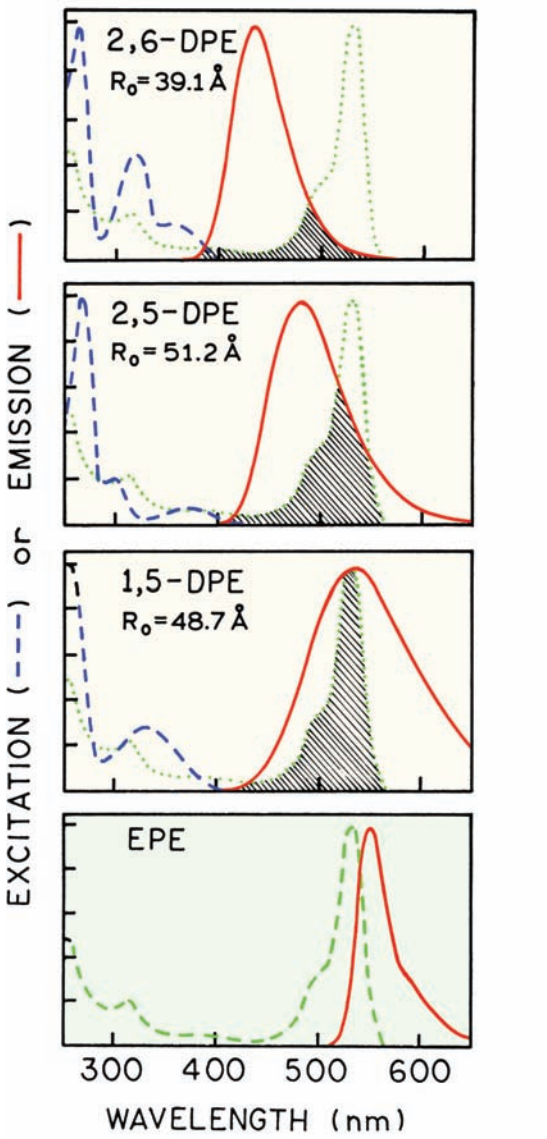

Figure 13.3. Excitation and emission spectra of dansyl-labeled lipids and an eosin-labeled lipid. The eosin- and dansyl-labeled compounds are N-derivatives of phosphatidylethanolamine (PE). The numbers refer to the location of the dimethylamino and the sulfonyl residues on the naphthalene ring. The extinction coefficient of EPE is 85,000 M^{-1} cm^{-1} at 527 nm. In the top three panels the long wavelength absorption spectrum of eosin–PE is shown as a dotted line. Revised and reprinted with permission from [5]. Copyright © 1978, American Chemical Society.

Table 13.1. Calculated R_0 Values for RET from Structural Isomers of Dansyl-Labeled Phosphatidylethanolamine (DPE) to Eosin-Labeled Phosphatidylethanolamine (EPE) and from 2,6-DPE to 2,5-DPE

Donor	Acceptor	Q_D	J (M^{-1} cm^3)	J (M^{-1} cm^3 $(nm)^4$)[d]	R_0 (Å)[a]
1,5-DPE[b]	EPE[c]	0.37	2.36×10^{-13}	2.36×10^{15}	48.7
2,5-DPE	EPE	0.76	1.54×10^{-13}	1.54×10^{15}	51.2
2,6-DPE	EPE	0.71	3.31×10^{-14}	3.31×10^{14}	39.1
2,6-DPE	2,5-DPE	0.71	1.3×10^{-15}	1.3×10^{13}	22.8

[a]From [5]. R_0 was calculated using $n = 1.4$ andy $\kappa^2 = 2/3$.

[b]Dansyl-labeled phosphatidylethanolamine.

[c]Eosin-labeled phosphatidylethanolamine.

[d]The factor of 10^{28} between $J(\lambda)$ in M^{-1} cm^3 and M^{-1} cm^3 $(nm)^4$ arises from 1 nm = 10^{-7} cm, raised to the fourth power.

fold change in the Förster distance. This is because of the sixth-root dependence in eq. 13.5. It should also be noted that the visual impression of overlap is somewhat misleading because the value of $J(\lambda)$ depends on λ^4 (eq. 13.3). Comparison of the spectral overlap for 2,5-DPE and 1,5-DPE suggests a larger Förster distance for 1,5-DPE, whereas the calculated value is smaller. The larger Förster distance for 2,5-DPE is due to its larger quantum yield. Because of the complexity in calculating overlap integrals and Förster distances it is convenient to have several examples. Values of the overlap integral corresponding to the spectra in Figure 13.3 are summarized in Table 13.1.

Brief History of Theodor Förster[8–9]

The theory for resonance energy transfer was developed by Professor Theodor Förster (Figure 13.4). He was born in Frankfurt, Germany in 1910. He received a PhD in 1933 for studies of the polarization of reflected electrons. He then became a Research Assistant in Leipzig, Germany, where he studied light absorption of organic compounds until 1942. In this phase of his work he applied the principles of quantum mechanics to chemistry. From 1942 to 1945 he held a Professorship in Poznan, Poland. In 1945 he joined the Max-Planck Institute for Physical Chemistry in Göttingen, where he wrote his classic book *Fluoreszenz Organischer Verbindungen*, which has been described as a "house bible" for the German community of spectroscopists. By 1946 Professor Förster had written his first paper on energy transfer, and pointed out the importance of energy transfer in photosynthesis systems. Professor Förster was also among the first scientists to observe excited-state proton transfer, which is now described by the Förster cycle. In 1954 he discovered excimer formation. Professor Förster died of a heart attack in his car on the way to work in 1974. For additional information see [8] and the introduction about Theodor Förster in [9].

13.2.1. Orientation Factor κ^2

A final factor in the analysis of the energy transfer efficiencies is the orientation factor κ^2 which is given by

$$\kappa^2 = (\cos\theta_T - 3\cos\theta_D\cos\theta_A)^2 \qquad (13.15)$$

$$\kappa^2 = (\sin\theta_D\sin\theta_A\cos\phi - 2\cos\theta_D\cos\theta_A)^2 \qquad (13.16)$$

In these equations θ_T is the angle between the emission transition dipole of the donor and the transition absorption dipole of the acceptor, θ_D and θ_A are the angles between these dipoles and the vector joining the donor and the acceptor, and ϕ is the angle between the planes (Figure

Figure 13.4. Professor Theodor Förster. 15 May 1910–20 May 1974. Reprinted with permission from [8]. Copyright © 1974, Springer-Verlag.

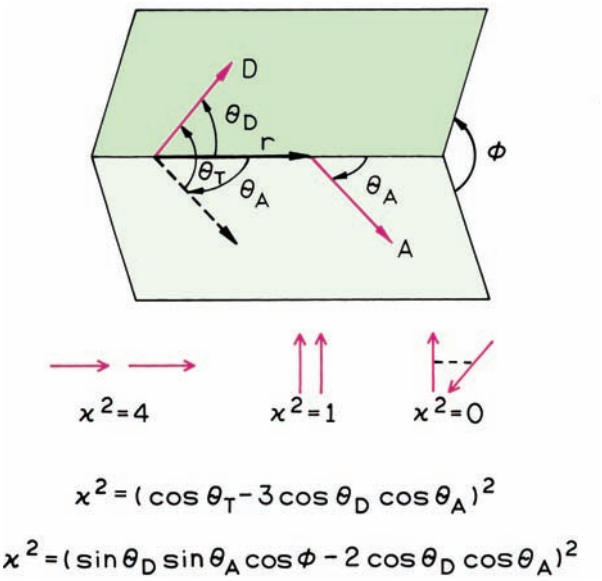

Figure 13.5. Dependence of the orientation factor κ^2 on the direction of the emission dipole of the donor and the absorption dipole of the acceptor.

13.5). Depending upon the relative orientation of donor and acceptor this factor can range from 0 to 4. For head-to-tail parallel transition dipoles $\kappa^2 = 4$, and for parallel dipoles $\kappa^2 = 1$. Since the sixth root is taken to calculate the distance, variation of κ^2 from 1 to 4 results in only a 26% change in r. Compared to $\kappa^2 = 2/3$, the calculated distance can be in error by no more than 35%. However, if the dipoles are oriented perpendicular to one another, $\kappa^2 = 0$, which would result in serious errors in the calculated distance. This problem has been discussed in detail.[10–12] By measurements of the fluorescence anisotropy of the donor and the acceptor, one can set limits on κ^2 and thereby minimize uncertainties in the calculated distance.[11–13] An example of calculating the range of possible values of κ^2 is given below. In general, variation of κ^2 does not seem to have resulted in major errors in the calculated distances.[14–15] κ^2 is generally assumed equal to 2/3, which is the value for donors and acceptors that randomize by rotational diffusion prior to energy transfer. This value is generally assumed for calculation of R_0. Alternatively, one may assume that a range of static donor–acceptor orientations are present, and that these orientations do not change during the lifetime of the excited state. In this case $\kappa^2 = 0.476$.[3] For fluorophores bound to macromolecules, segmental motions of the donor and acceptor tend to randomize the orientations. Further, many donors and acceptors display fundamental anisotropies less than 0.4 due to overlapping electronic transitions. In this case the range of possible κ^2 values is more limited, and errors in distance are likely to be less than 10%.[16] Experimental results on the effect of κ^2 are given in Section 13.9.

13.2.2. Dependence of the Transfer Rate on Distance (r), the Overlap Integral (J), and τ^2

The theory of Förster predicts that $k_T(r)$ depends on $1/r^6$ (eq. 13.1) and linearly on the overlap integral (eq. 13.2). Given the complexity and assumptions of RET theory,[4] it was important to demonstrate experimentally that these dependencies were valid. The predicted $1/r^6$ dependence on distance was confirmed experimentally.[17–19] One demonstration used oligomers of poly-L-proline, labeled on opposite ends with a naphthyl (donor) and a dansyl (acceptor) group.[17–18] Poly-L-proline forms a rigid helix of known atomic dimensions, providing fixed distances between the donor and acceptor moieties. By measuring the transfer efficiency with different numbers of proline residues, it was possible to demonstrate that the transfer efficiency in fact decreased as $1/r^6$. These data are described in detail in Problem 13.3.

The linear dependence of $k_T(r)$ on the overlap integral $J(\lambda)$ has also been experimentally proven.[20] This was accomplished using a D–A pair linked by a rigid steroid spacer. The extent of spectral overlap was altered by changing the solvent, which shifted the indole donor emission spectrum and the carbonyl acceptor absorption spectra. The rate of transfer was found to decrease linearly as the overlap integral decreased. These data are shown in Problem 13.4. To date there has not been experimental confirmation of the dependence of the transfer rate on κ^2.

Another important characteristic of RET is that the transfer rate is proportional to the decay rate of the fluorophore (eq. 13.2). This means that for a D–A pair spaced by the R_0 value, the rate of transfer will be $k_\tau(r) = \tau_D^{-1}$ whether the decay time is 10 ns or 10 ms. Hence, long-lived lanthanides are expected to display RET over distances comparable to those for nanosecond-decay-time fluorophores, as demonstrated by transfer from Tb^{3+} to acceptor.[21–23] This fortunate result occurs because the transfer rate is proportional to the emission rate of the donor. The proportionality to the emissive rate is due to the term Q_D/τ_D in eq. 13.2. It is interesting to speculate what would happen if the transfer rate was independent of the decay rate. In this case a longer lived donor would allow more time for energy transfer. Then energy transfer would occur over longer

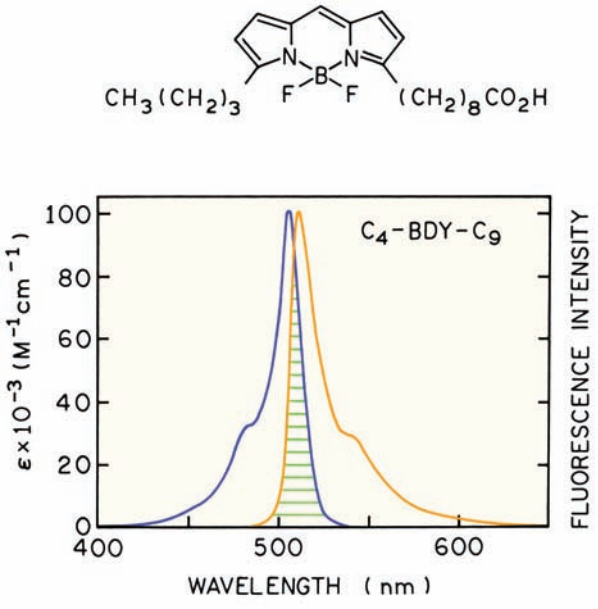

Figure 13.6. Absorption and corrected fluorescence emission (band-pass 2.5 nm) spectra of the Bodipy derivative C_4-BDY-C_9 in methanol with shaded area representing spectral overlap. Revised and reprinted with permission from [25]. Copyright © 1991, Academic Press, Inc.

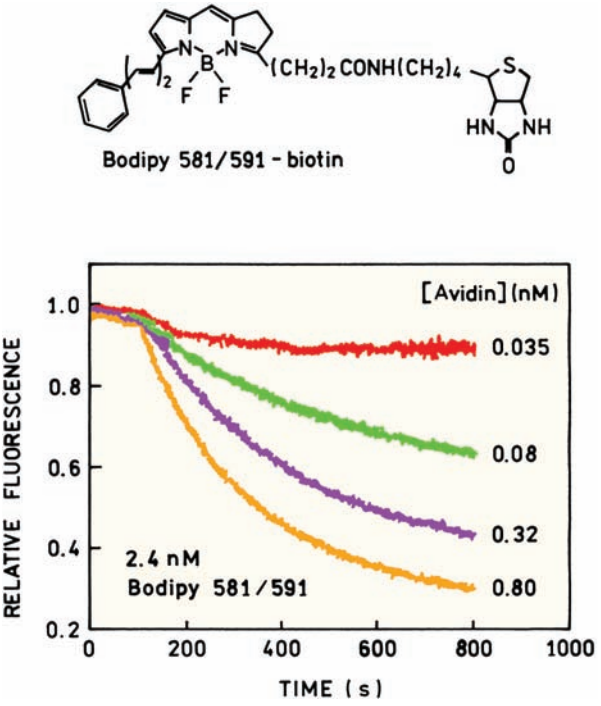

Figure 13.7. Self-quenching of Bodipy 581/591-biotin upon binding to avidin. Revised from [30].

distances because a smaller rate of transfer will still be comparable to the donor decay rate.

13.2.3. Homotransfer and Heterotransfer

In the preceding sections we considered only energy transfer between chemically distinct donors and acceptors, which is called heterotransfer. Resonance energy transfer can also occur between chemically identical molecules. Such transfer, which is termed homotransfer, typically occurs for fluorophores which display small Stokes shifts. One example of homotransfer is provided by the Bodipy fluorophores.[24] The absorption and emission spectra of one Bodipy derivative are shown in Figure 13.6. Because of the small Stokes shift and high extinction coefficient of these probes, the Förster distance for homotransfer is near 57 Å.[25]

At first glance homotransfer may seem like an unlikely phenomenon, but its occurrence is rather common. For example, it is well known that biomolecules labeled with fluorescein do not become more highly fluorescent with higher degrees of labeling.[26–28] Antibodies are typically brightest with about four fluoresceins per antibody, after which the intensity starts to decrease. This effect is attributed to the small Stokes shift of fluorescence and homotransfer. In fact, homotransfer among fluorescent molecules was one of the earliest observations in fluorescence, and was detected by a decrease in the anisotropy of fluorophores at higher concentrations.[29] The possibility of homotransfer can be readily evaluated by examination of the absorption and emission spectra. For instance, perylene would be expected to display homotransfer but homotransfer is unlikely in quinine (Figure 1.3).

It is informative to see an example of self-quenching. Figure 13.7 shows the emission intensity of Bodipy 581/591-biotin upon the addition of avidin.[30] In the Bodipy probes the numbers refer to the excitation and emission wavelength, but these are only approximate values. Avidin is a tetramer with four binding sites for biotin. It is a relatively large protein about 50 Å is diameter. The biotin binding sites are about 30 Å apart. Before addition of avidin there is no self-quenching of Bodipy because the fluorophores are too far apart in this nM solution. Upon addition of avidin the Bodipy intensity decreases. There is little change in intensity when the avidin concentration is low: 0.035 mM. At this concentration there is not enough avidin to bind more than a small fraction of the Bodipy. At an avidin concentration of 0.8 nM there are about 3 Bodipy probes bound per avidin and the Bodipy is 70% quenched. The fact that Bodipy is quenched shows that the R_0 value for

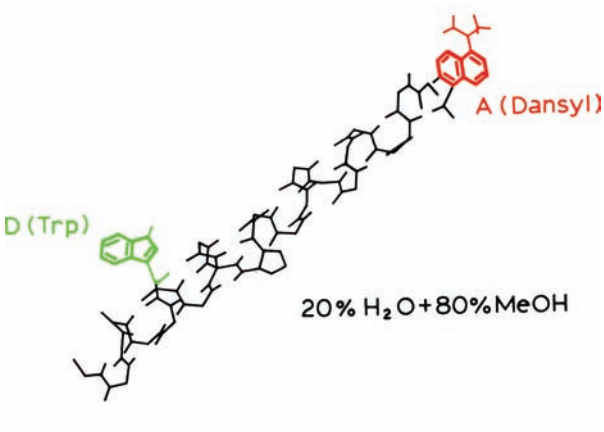

Figure 13.8. Chemical structure of melittin in the α-helical state. The donor is tryptophan-19 and the acceptor is a N-terminal dansyl group. Revised from [31].

homotransfer is at least as large as the 30 Å distance between the binding sites.

13.3. DISTANCE MEASUREMENTS USING RET

13.3.1. Distance Measurements in α-Helical Melittin

Since resonance energy transfer can be reliably assumed to depend on $1/r^6$, the transfer efficiency can be used to measure distances between sites in proteins. The use of RET in structural biochemistry is illustrated in Figure 13.8 for the peptide melittin.[31] This peptide has 26 amino acids. A single-tryptophan residue at position 19 serves as the donor. A single-dansyl acceptor was placed on the N-terminal amino group. The spectral properties of this D–A pair are shown in Figure 13.9. These spectral properties result in a Förster distance of 23.6 Å (Problem 13.5).

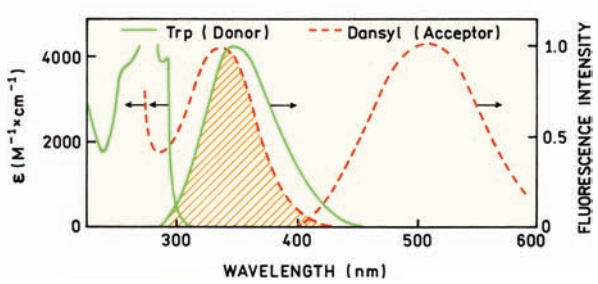

Figure 13.9. Overlap integral for energy transfer from a tryptophan donor to a dansyl acceptor on melittin R_0 = 23.6 Å. Data from [31].

Depending on the solvent conditions melittin can exist in the monomer, tetramer, α-helix, and/or random coil state.[32–33] In the methanol–water mixture specified on Figure 13.8 melittin is in the rigid α-helical state and exists as a monomer. There is a single-dansyl acceptor adjacent to each tryptophan donor, and the helical structure ensures a single D–A distance, except for the range of distances allowed by the flexing side chains. Hence, we can use the theory described above, and in particular eqs. 13.12 and 13.13, to calculate the D–A distance.

In order to calculate the D–A distance it is necessary to determine the efficiency of energy transfer. This can be accomplished by comparing the intensity of the donor in the presence of acceptor (F_{DA}), with the donor intensity from a control molecule which lacks the acceptor (F_D). From Figure 13.10 one sees that the value of F_{DA}/F_D is near 0.55, so that the transfer efficiency is less than 50%: $E = 0.45$. Since E is less than 0.5 we know that the D-to-A distance must be larger than the R_0 value. Using eq. 13.12 and an R_0 value of 23.6 Å, one can readily calculate that the tryptophan-to-dansyl distance is 24.4 Å.

It is important to remember the assumptions used in calculating the distance. We assumed that the orientation factor κ^2 was equal to the dynamic average of 2/3. In the case of melittin this is a good assumption because both the trp donor and dansyl acceptor are fully exposed to the liquid phase which is highly fluid. The rotational correlation times for such groups is typically near 100 ps, so that the dipoles can randomize during the excited-state lifetime.

Another assumption in calculating the trp to dansyl distance in melittin is that a single conformation exists, that there is a single D–A distance. This assumption is probably

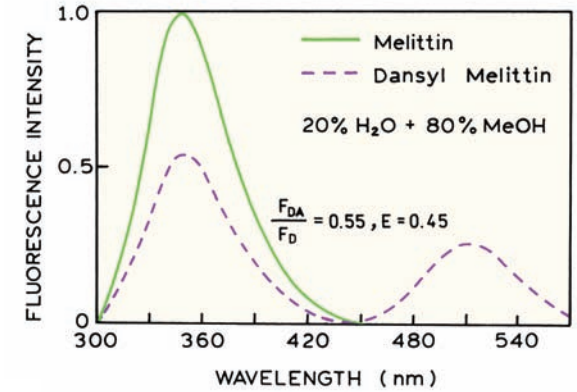

Figure 13.10. Emission spectra of the melittin donor (D) and acceptor-labeled melittin (D–A). Excitation at 282 nm. Revised from [31].

safe for many proteins in the native state, particularly for single-domain proteins. For unfolded peptides or multi-domain proteins a variety of conformations can exist, which results in a range of D–A distances. In this case calculation of a single distance using eq. 13.12 would result in an apparent distance, which would be weighted towards the shorter distances. Such systems are best analyzed in terms of a distance distribution using the time-resolved data (Chapter 14).

13.3.2. Effects of Incomplete Labeling

The largest source of error in calculating distance from the RET data is probably incomplete labeling with the acceptor. If melittin were incompletely labeled with acceptor, the measured value of F_{DA} would be larger than the true value, and the calculated distance too large. We are less concerned with underlabeling by the donor because the protein molecules that do not contain donors do not contribute to the donor intensity, assuming the extent of donor labeling is the same for the donor-alone and donor–acceptor pair.

If the fractional labeling with donor (f_a) is known then the relative intensities can be used to calculate the transfer efficiency. In this case eq. 13.14 becomes[13]

$$E = 1 - \frac{F_{DA} - F_D(1 - f_A)}{F_D f_A} = \left(1 - \frac{F_{DA}}{F_D}\right)\frac{1}{f_A} \quad (13.17)$$

For a high degree of RET donor quenching, ($F_{DA}/F_D << 1$), a small percentage of unlabeled acceptor can result in a large change in the calculated transfer efficiency (Problem 13.9). The effect of $f_a < 1.0$ is shown in Figure 13.11. Subfragment S-1 myosin, Myosin S-1, contains 42 thiol groups, two of which are highly reactive. These groups were labeled with 1,5-IAEDANS as the donor and IAF as the acceptor.[34] The transfer efficiency can be calculated from the relative intensities of the donor at 475 nm in the donor-alone or D–A pair. This yields a transfer efficiency of 30%. Since the Förster distance for this D–A pair is about 30 Å, the calculated distance between the D and A is 49 Å. However, the sample shown in Figure 13.11 was incompletely labeled with acceptor, so that $f_a = 0.50$. Using eq. 13.17 yields a transfer efficiency of 60% and a D–A distance of 40 Å. Hence it is essential to obtain complete labeling with the acceptor or to know the extent of acceptor labeling.

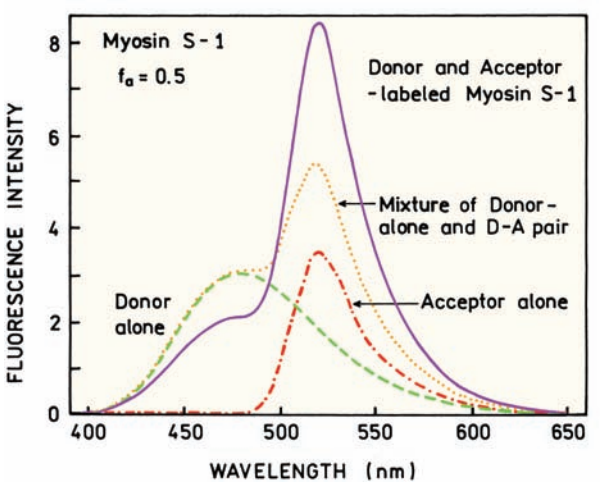

Figure 13.11. Emission spectra of labeled Myosin S-1. The donor is 1,5-IAEDANS and the acceptor is IAF. Revised from [34].

13.3.3. Effect of κ^2 on the Possible Range of Distances — Advanced Topic

In distance measurements using RET there is often concern about the effects of the orientation factor κ^2. At present there is no way to measure κ^2, except by determination of the x-ray crystal structure, or NMR structure, in which case the distance would be known and thus there would be no reason to use energy transfer. However, it is possible to set limits on κ^2 that in turn set limits on the range of possible D–A distances. These limits are determined from the anisotropies of the donor and acceptor, which reflects the extent of orientational averaging toward the dynamic average of $\kappa^2 = 2/3$.

The problem of κ^2 has been discussed in detail by Dale and coworkers[10–12] and summarized by Cheung.[13] The basic idea is that the donor and acceptor move freely within a cone and that energy transfer is rapidly averaged over all available D–A orientations. Interpretation of the formalism described by Dale and coworkers is not always straightforward, and we present the method preferred in this laboratory.[35] While it is not possible to calculate the values of κ^2, it is possible to set upper and lower limits. These values are given by

$$\kappa^2_{min} = \frac{2}{3}\left[1 - \frac{(d^x_D + d^x_A)}{2}\right] \quad (13.18)$$

$$\kappa^2_{max} = \frac{2}{3}(1 + d^x_D + d^x_A + 3d^x_D d^x_A) \quad (13.19)$$

where

$$d_i^x = (r_i/r_0)^{1/2} \tag{13.20}$$

The value of d_i^x represents the depolarization factor due to segmental motion of the donor (d_D^x) or acceptor (d_A^x), but not the depolarization due to overall rotational diffusion of the protein. Overall rotational diffusion is not important because it does not change the D–A orientation. The values of r_i and r_0 are often taken as the steady-state and fundamental anisotropies of the donor or acceptor. If the donor and acceptor do not rotate relative to each other during the excited-state lifetime, then $d_D^x = d_A^x = 1.0$, and $\kappa_{min}^2 = 0$ and $\kappa_{max}^2 = 4$. If both D and A are independently and rapidly rotating over all space, $\kappa_{min}^2 = \kappa_{max}^2 = 2/3$.

There are several ways to obtain the values of d_D^x and d_A^x. The easiest method is to determine the anisotropy decays of the donor and acceptor, the latter when directly excited. This calculation of a range of κ^2 values is illustrated by the anisotropy decays measured for the tryptophan donor and dansyl acceptor in α-helical melittin (Table 13.2). Both the donor and the acceptor display two correlation times, one due to overall protein rotation near 2 ns, and a shorter correlation time near 0.3 ns due to segmental motions of the donor and the acceptor. It is these faster motions that randomize κ^2. The values of d_D^x and d_A^x are given by the ratio of the long correlation time amplitude to the total anisotropy. Hence, for melittin

$$d_D^x = \left(\frac{0.174}{0.294}\right)^{1/2} = 0.77 \tag{13.21}$$

$$d_A^x = \left(\frac{0.135}{0.300}\right)^{1/2} = 0.67 \tag{13.22}$$

Using these values and eqs. 13.18 and 13.19 one can calculate the limits on κ^2, $\kappa_{min}^2 = 0.19$, and $\kappa_{max}^2 = 2.66$.

Table 13.2. Anisotropy Decays for α-Helical Melittin[a]

Fluorophore	r_{0i}	θ_i (ns)
Tryptophan 19[b]	0.120	0.23
	0.174	1.77
N-terminal dansyl	0.165	0.28
	0.135	2.18

[a]From [31].

[b]Determined for donor-only melittin. Similar amplitudes and correlation times were found for trp-19 in dansyl melittin.

Once the limiting values of κ^2 are known one may use these values to calculate the maximum and minimum values of the distance which are consistent with the data. In calculating these distances one must remember that R_0 was calculated with an assumed value of $\kappa^2 = 2/3$. Hence the minimum and maximum distances are given by

$$r_{min} = \left(\frac{\kappa_{min}^2}{2/3}\right)^{1/6} r\left(\kappa^2 = \frac{2}{3}\right) \tag{13.23}$$

$$r_{max} = \left(\frac{\kappa_{max}^2}{2/3}\right)^{1/6} r\left(\kappa^2 = \frac{2}{3}\right) \tag{13.24}$$

where $r(\kappa^2 = 2/3)$ is the distance calculated assuming $\kappa^2 = 2/3$. Using the limiting values of κ^2 one finds for the example given above that the distance can be from 0.81 to 1.26 of $r(\kappa^2 = 2/3)$. While this difference may seem large it should be remembered that there is an additional depolarization factor due to the transfer process itself, which will further randomize κ^2 towards 2/3. Equations 13.18–13.20 provide a worst-case estimate, which usually overestimates the effects of κ^2 on the calculated distance. For fluorophores with mixed polarization, where $r_0 < 0.3$, the error in distance is thought to be below 10%.[16]

There are two other ways to obtain the depolarization factors. One method is to construct a Perrin plot in which the steady-state polarization is measured for various viscosities. Upon extrapolation to the high-viscosity limit, the $1/r_{app}$ intercept (Chapter 10) is typically larger than $1/r_0$ in frozen solution. This difference is usually attributed to segmental probe motions, and can be used to estimate the depolarization factor, $d_i^x = (r_{app}/r_0)^2$. Another method is to estimate the expected steady-state anisotropy from the lifetime and correlation time of the protein, and to use these data to estimate d_D^x and d_A^x (Problem 13.8). The basic idea is to estimate d_A^x and d_D^x by correcting for the decrease in anisotropy resulting from rotational diffusion of the protein. Any loss in anisotropy, beyond that calculated for overall rotation, is assumed to be due to segmental motions of the donor or acceptor.

13.4. BIOCHEMICAL APPLICATIONS OF RET

13.4.1. Protein Folding Measured by RET

In many experiments it is not necessary to calculate the distances because the biochemical question can be answered

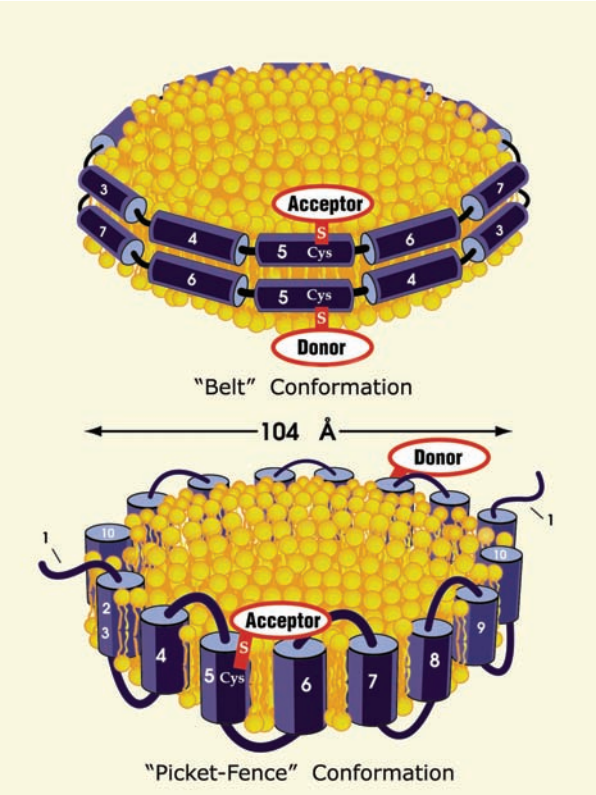

Figure 13.12. Possible conformations for apolipoprotein apoA-I when bound to lipids. Reprinted with permission from [36]. Figure courtesy of Dr. Mary G. Sorci-Thomas from the Wake Forest University, N.C.

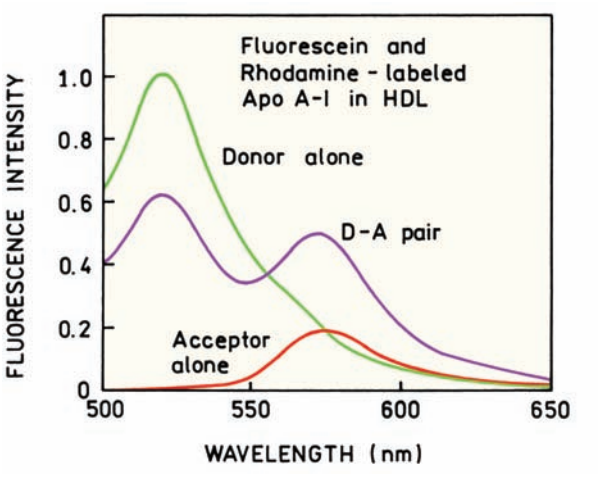

Figure 13.13. Emission spectra of labeled apoA-I in HDL. Revised from [36].

from the presence or absence of RET. One example of this approach is determination of the conformation of an apolipoprotein when bound to lipids.[36] Apolipoproteins regulate cholesterol metabolism. ApoA-I is one of the most effective activators of lecithin:cholesterol acyltransferase (LCAT), which results in the formation of a discoidal form of high density lipoprotein (HDL). It is difficult to obtain x-ray structures from such proteins, and the conformation of the lipid-bound protein was uncertain. There were two possible structures (Figure 13.12). ApoA-I could form a belt around the lipid disk. Alternatively, apoA-I could fold as antiparallel α-helices in a picket fence conformation.

The problem of the apoA-I conformation was addressed using RET. Recombinant apoA-I was made with a cysteine substituted for a glutamine at position 132, the Q132C mutant. It was known that the discoidal complex contained two molecules of apoA-I. One batch of apoA-I was labeled with the sulfhydryl-reactive fluorescein 5-IAF, and the other batch labeled with a sulfhydryl-reactive tetramethylrhodamine. Figure 13.13 shows emission spectra of labeled apoA-I in discoidal HDL. The spectrum of the D–A pair shows a decrease in donor intensity and an increase in acceptor intensity, consistent with about 40% energy transfer. The presence of RET proves that apoA-I is in the belt conformation (Figure 13.12) because RET would not occur for the picket-fence conformation where the donor and acceptor are 104D apart. Other groups agree with the belt structure, but believe the peptides are in a hairpin conformation.[37]

It is interesting to notice that the question was answered in spite of some complexity. Each discoidal particle could contain two donors, two acceptors, or one of each. The spectra in Figure 13.13 were obtained with a threefold excess of acceptor, so that most of the donors had a nearby acceptor. However, it was not necessary to resolve these populations to determine the confirmation of apoA-I in these particles. Additional references on RET and protein folding are listed near the end of the chapter.

13.4.2. Intracellular Protein Folding

RET with intensity ratio measurements have also been used to study protein folding in cells. Another apolipoprotein, apo E4, is associated with Alzheimer's disease. Apo E4, found in neurofibrillary tangles and amyloid plaques, is known to modulate plaque formation, and binds to very low density lipoproteins. Apo E3 has a similar amino acid sequence but binds to high-density lipoproteins and is not thought to be involved in amyloid protein deposition.

The different physiological effects of apo E4 and apo E3 are thought to be due to the different interactions

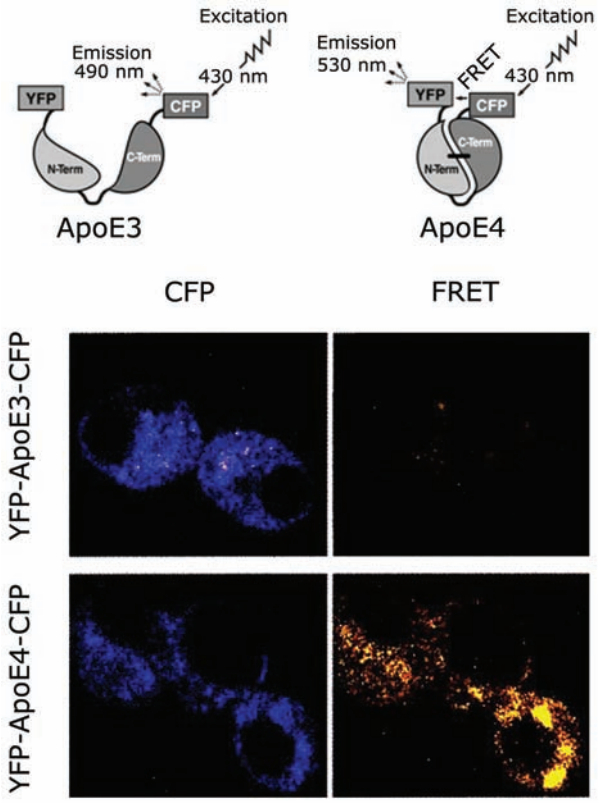

Figure 13.14. Schematic of labeled Apo E3 and Apo E4, and donor (CFP) and RET images in Neuro-2a cells. Reprinted with permission from [38].

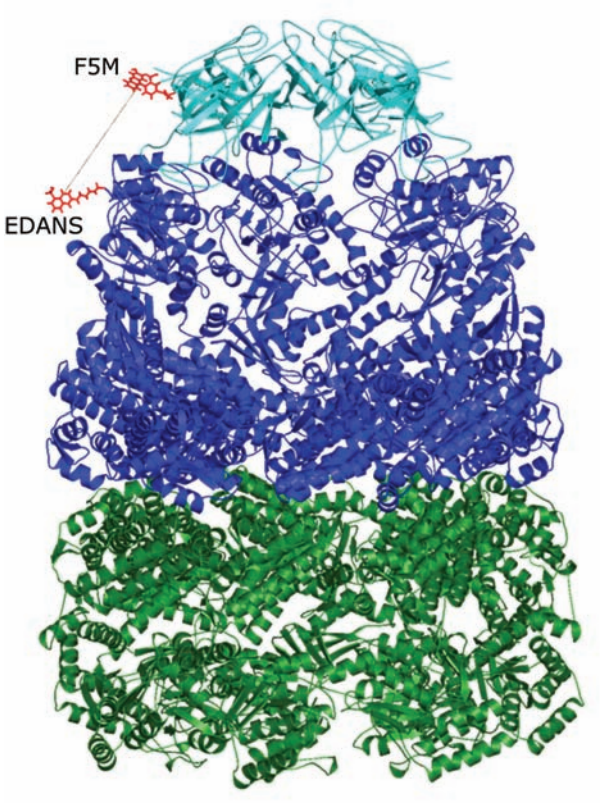

Figure 13.15. Structure of GroEL (green and blue) and GroES (light blue). The red structures are the donor and acceptor. Revised from [42]. Courtesy of Dr. Hays S. Kye from the Princeton University, N.J.

between their two domains. Hence it was of interest to look for association of the domains in neuronal cells (Figure 13.14). The neuronal cells, Neuro-2a, were transfected with the constructs encoding for apo E4 or apo E3 that contained an energy-transfer pair of CFP (donor) and YFP (acceptor). The extent of RET was expected to depend on domain association. Donor images of the cells showed that the protein was expressed and was localized mostly in the cytoplasm. Taking ratios of the donor and acceptor images showed that RET occurred for intracellular apo E4 but not for intracellular apo E3. These results demonstrate how the applications of RET are being expanded to include in-vivo imaging.

13.4.3. RET and Association Reactions

RET can be used to measure binding interactions between molecules in solution[39] or in microscopy.[40–41] RET was used to detect association of the chaperonin proteins GroEL and GroES[42]. GroEL is a 798-kilodalton protein containing 57 identical subunits. The subunits form a large barrel that facilitates refolding of proteins. This process requires binding of the 70-kilodalton CAP GroES (Figure 13.15). Binding of these two complexes depends on the presence of ATP.

Binding between GroEL and GroES was measured using RET. Mutant proteins were made with single-cysteine residues for labeling. GroEL was labeled with 2,5-IEDANS and GroES with a fluorescein derivative. Emission spectra of each protein and a mixture are shown in Figure 13.16. The spectrum from the mixture, in the absence of ATP (top), is the sum of the individual spectra. The result shows that GroEL and GroES are not bound together in the absence of ATP. Addition of ATP resulted in a decrease in the donor emission and an increase in the acceptor emission (bottom), which is due to formation of the GroEL–GroES complex.

RET was used to follow binding kinetics. Figure 13.17 shows the effect of adding unlabeled GroES to the complex. In the presence of ATP the complexes dissociate and reassociate, which may occur during refolding of proteins. As

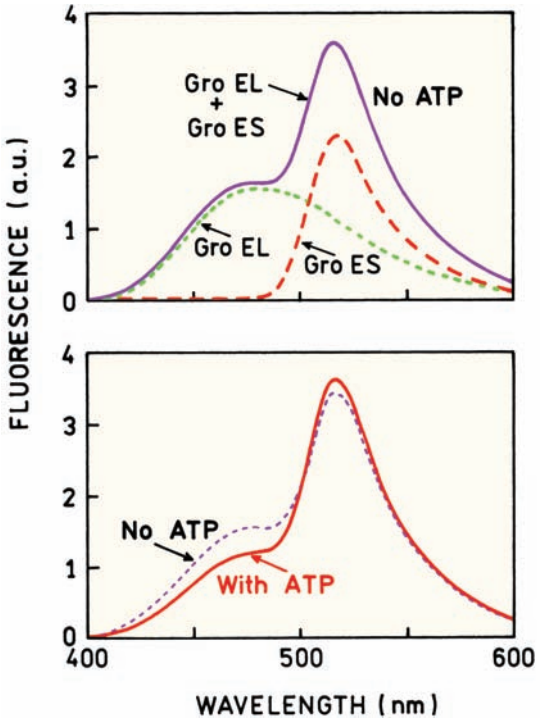

Figure 13.16. Emission spectra of IEDANS-labeled GroEL and fluorescein-labeled GroES without (top) and with (bottom) ATP. Revised from [42].

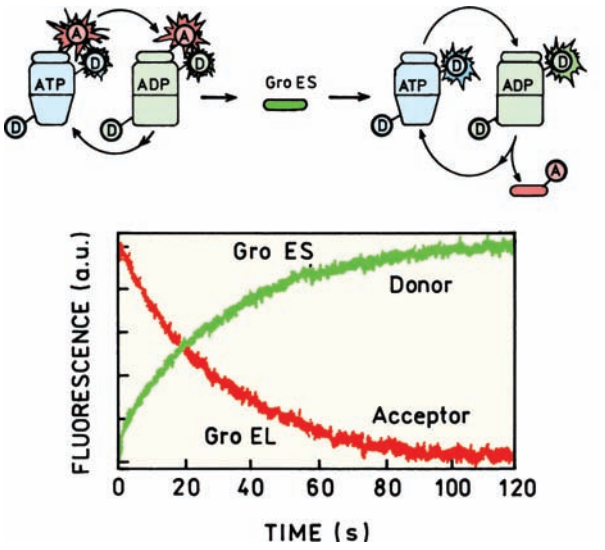

Figure 13.17. Dissociation of doubly labeled GroEL–GroES. Revised from [42].

unlabeled GroES associates with labeled GroEL the donor intensity increases and the acceptor intensity decreases. This result shows that information about binding can be obtained using either the donor or acceptor emission.

13.4.4. Orientation of a Protein-Bound Peptide

In the presence of calcium, calmodulin is known to interact with a number of proteins and peptides. For example, a peptide from myosin light-chain kinase (MLCK) binds to calmodulin.[43] Such peptides are known to bind in the cleft between the two domains of calmodulin (Figure 13.18). When bound to calmodulin the MLCK peptide was known to adopt a α-helical conformation. However, the direction of peptide binding to calmodulin was not known.

Information on the direction of binding was obtained by studying of four similar peptides, each containing a single-tryptophan residue that served as the donor (Figure 13.19). Calmodulin typically contains only tyrosine residues, so an intrinsic acceptor was not available. This problem was solved by using calmodulin from spinach, which contains a single-cysteine residue at position 26. This residue was labeled with 1,5-IAEDANS, which contains a thiol-reactive iodoacetyl group. The Förster distances for trp-to-AEDANS energy transfer ranged from 21 to 24 Å.

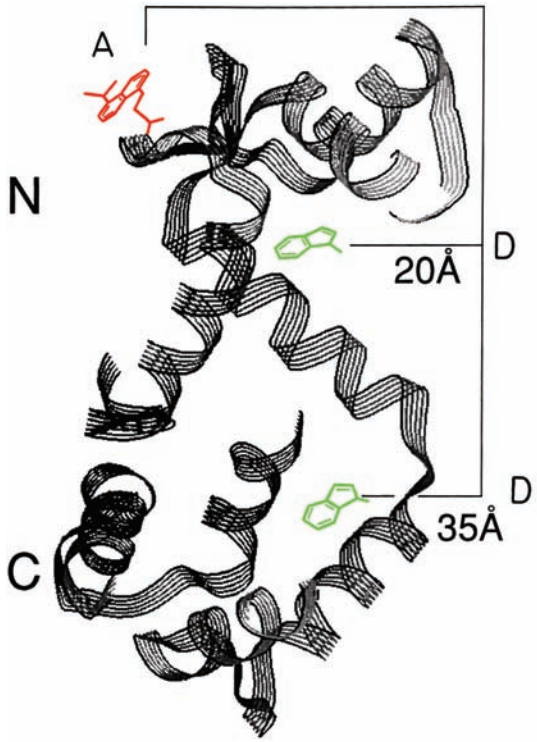

Figure 13.18. Structure of spinach calmodulin. The acceptor is AEDANS on cysteine-26 of calmodulin. The tryptophan donor is on the myosin light chain kinase peptides shown in Figure 13.19. Revised and reprinted with permission from [43]. Copyright © 1992, American Chemical Society.

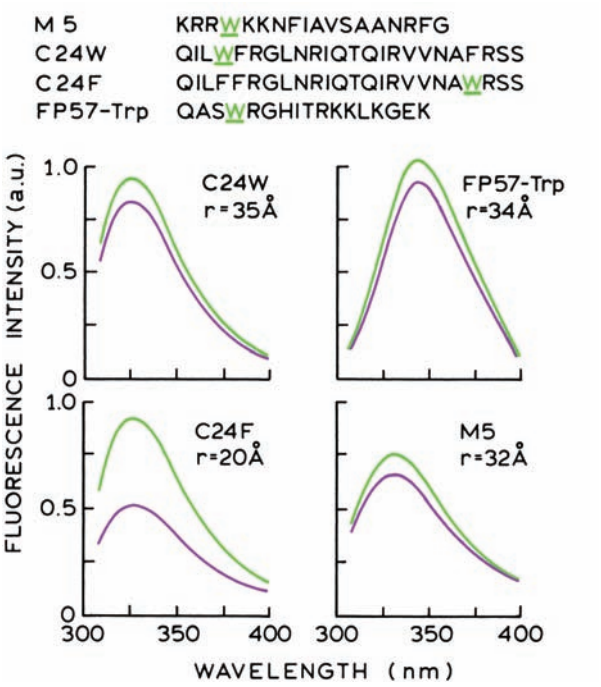

Figure 13.19. Emission spectra of the MLCK peptides when free in solution and when bound to AEDANS-calmodulin. The upper and lower spectra correspond to the peptide emission spectra in the absence and presence of AEDANS-calmodulin, respectively. The peptide sequences are shown in the top panel, and the calculated distance shown with the spectra. Excitation at 295 nm. Revised and reprinted with permission from [43]. Copyright © 1992, American Chemical Society.

Emission spectra of the tryptophan-containing peptides are shown in Figure 13.19. The excitation wavelength was 295 nm to avoid excitation of the tyrosine residues in calmodulin. Upon binding of AEDANS–calmodulin the tryptophan emission of each peptide is quenched. One of the peptides showed a transfer efficiency of 54%, and the remaining three peptides showed efficiencies ranging from 5 to 16%. These results demonstrated that the C-terminal region of the peptides bound closely to the N-terminal domain of calmodulin, and illustrate how structural information can be obtained by comparative studies of analogous structures.

13.4.5. Protein Binding to Semiconductor Nanoparticles

Semiconductor nanoparticles, or Quantum Dots (QDs), have become widely used as fluorescent probes. They can have high quantum yields, narrow emission spectra, and good photostability (Chapter 3). Understanding the interactions of Quantum Dots with proteins is important for their use as intracellular probes and for making the surfaces functional. RET has been used to determine the interaction of the *E. coli* maltose-binding protein (MBP) when bound to a QD.[44]

The orientation of MBP when bound to a QD was determined using six single-cysteine mutants of MBP. The individual proteins were labeled with Rhodamine Red (RR) at the sites shown in the top panel of Figure 13.20. The QDs were then titrated with the RR-labeled MBP. The donor was the QDs with a diameter near 60 Å and emitting at 555 nm. Binding of RR–MBP resulted in quenched QD emission and increased RR emission (middle panels). For some of the MBP mutants strong donor quenching was observed, for

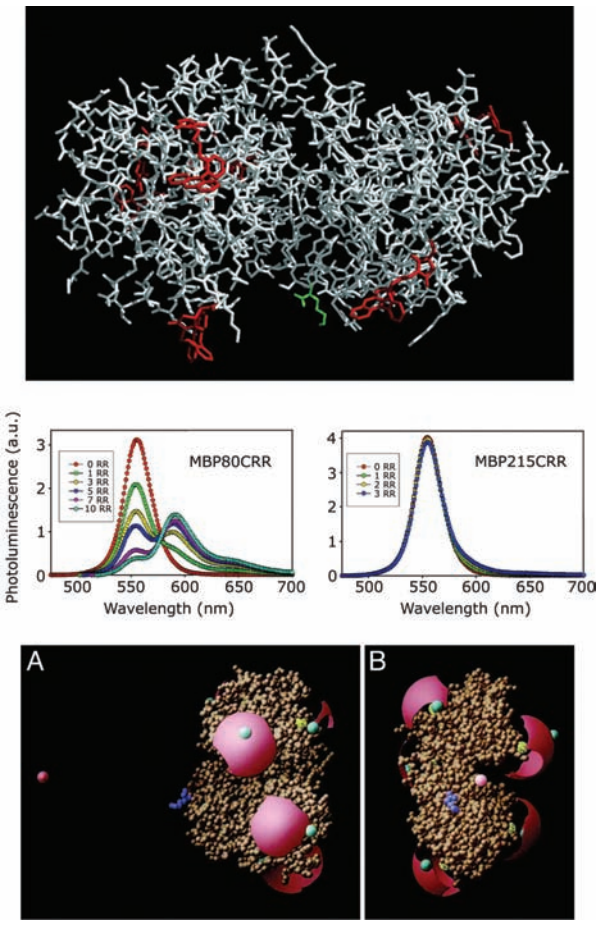

Figure 13.20. **Top**: *E. coli* malliose-binding protein shows six sites where Rhodamine Red was bound. **Middle**: Emission spectra of the QDs titrated with two RR-MBP. **Bottom**: Orientation of bound MBP relative to the center of the QD (pink dot). Revised from [44].

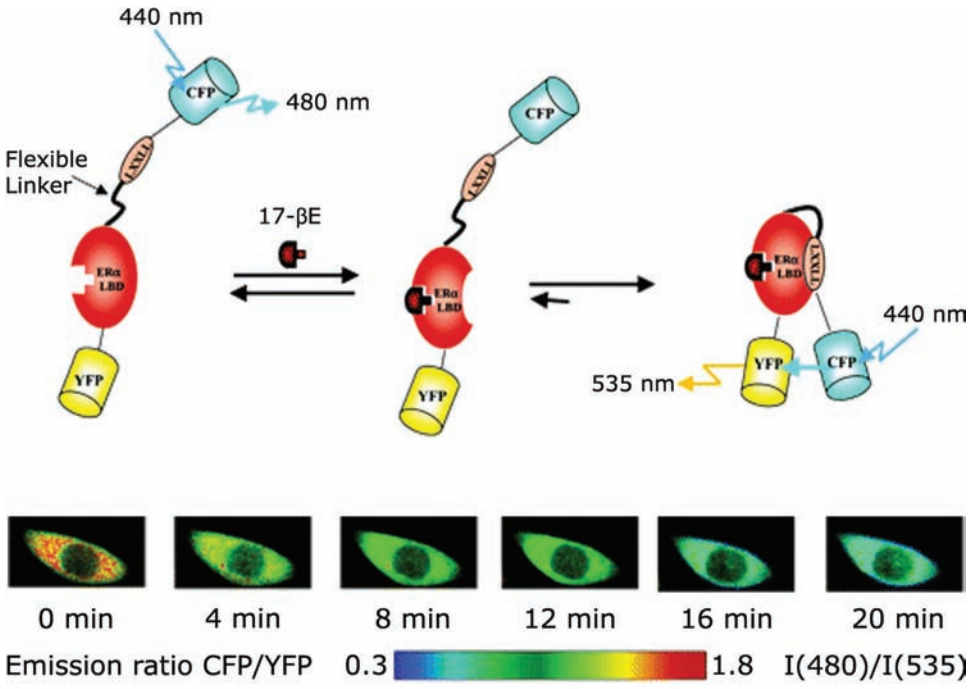

Figure 13.21. RET indicator for estrogens using the ligand-binding domain of estrogen receptor. The color scale shows the intensity at 480 nm divided by the intensity at 535 nm. Revised and reprinted with permission from [45]. Copyright © 2004, American Chemical Society.

other mutants there was almost no RET. By examination of the six mutant proteins the orientation of MBP on the surface of the a QD could be determined (Figure 13.20, lower panel). The center of the QD is shown as a pink dot, but the QD itself is not shown.

13.5. RET SENSORS

Resonance energy transfer has been used to develop a number of sensors. The use of donor-to-acceptor intensity ratios is valuable because the measurements become mostly independent of the overall intensity. This independence is especially important in fluorescence microscopy, where it is usually not possible to know or control the local fluorophore concentration.

13.5.1. Intracellular RET Indicator for Estrogens

RET has been used with green fluorescent proteins (GFPs) and their variants to develop sensors for a variety of analytes. One example is an intracellular indicator for estrogens.[45] In this case cyan (CFP) and yellow (YFP) fluorescent proteins form the RET pair (Figure 13.21). These proteins are linked by a peptide containing both the ligand-binding domain of estrogen receptor α (ER) and an estrogen-dependent ER-interaction site. The latter domain is comprised of the sequence LXXLL, where L is leucine and X is any other amino acid. Upon binding the ER against 17-β estradiol, the ER ligand-binding domain becomes competent to interact with the LXXLL motif. The resulting conformational change brings the tethered CFP and YFP moieties into close proximity, thus increasing the efficiency of energy transfer.

An advantage of using a GFP and its mutants is the potential to express the indicator in the cell rather than injecting or loading the indicator into the cell. A plasmid expression vector encoding the RET indicator was transfected into CHO cells, which then synthesized the indicator. The labeled cells were exposed to 17-βE and imaged at the emission wavelength of CFP (480 nm) and YFP (535 nm). The ratio of intensities was used to create a false color image of the cells (Figure 13.21). After exposure to 17-βE the intensity at 535 nm increased, while the intensity at 480 nm decreased. This approach allows cell-based assays for estrogen potency or the blocking effects of estrogen antagonists.

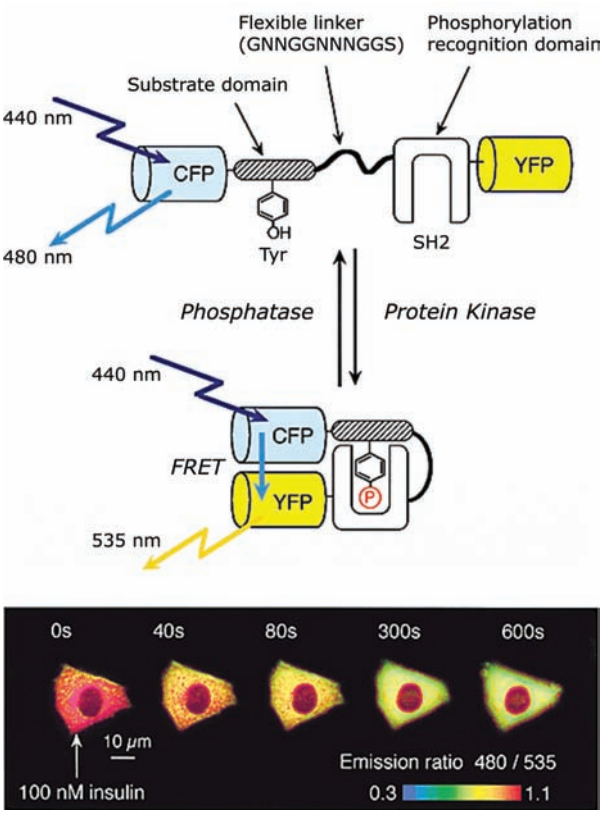

Figure 13.22. RET sensor for protein phosphorylation. Revised from [46].

13.5.2. RET Imaging of Intracellular Protein Phosphorylation

Protein phosphorylation by kinases is an important method of intracellular signaling. For example, the insulin receptor is a tyrosine kinase. The insulin receptor phosphorylates a tyrosine residue in a particular sequence, which then binds to a recognition domain (SH2) of another protein (Figure 13.22). This binding event brings CFP and YFP into closer proximity for increased RET. This protein was expressed in CHO-IR cells, which overexpress the insulin receptor. These transfected cells were then exposed to 100-nM insulin, which caused a time-dependent decrease in the donor-to-acceptor intensity ratio, which indicated an increase in RET. Ratiometric RET imaging can thus be used to study a wide variety of intracellular processes.

13.5.3. Imaging of Rac Activation in Cells

In the previous example the donor and acceptor proteins were covalently linked. Intracellular RET indicators can also be made when the donor and acceptor are not covalently linked but associate in the cell. The Rac is a GTPase that is involved in several processes, including actin dynamics and control of cell morphology. An approach for sensing Rac activation is shown in Figure 13.23. The donor was Rac–GFP. The acceptor was a kinase (PBD) labeled with Alexa-546. In the presence of GTP the labeled kinase PBD binds to Rac–GTP, as can be seen from the changes in the donor and acceptor intensities for these proteins in solution.[47] Assessment of this interaction in living cells was accomplished by transfection of the gene encoding Rac–GFP and microinjection of the labeled kinase. The confluent monolayer of cells was then scraped. This caused activation of Rac as the cells moved toward the open area and actin polymerization increases. The location-dependent concentrations of Rac–GFP are seen from the donor intensity images (Figure 13.24, right). An increase in RET, or binding of Rac–GFP to PBD, is seen as the shift from blue to green in the pseudocolor images (Figure 13.24, left). Comparison of the RET images with the GFP intensity images shows that the D–A intensity ratios are independent of the Rac–GFP concentration.

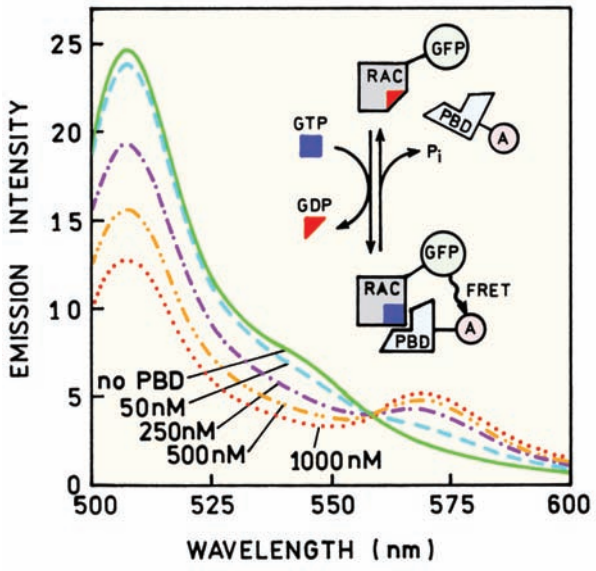

Figure 13.23. Emission spectra of Rac–GFP in the presence of GTP and an Alexa-546 labeled kinase (PBD) that binds to Rac. The value of R_0 is 51D. Revised from [47].

13.6. RET AND NUCLEIC ACIDS

RET is used extensively in DNA analysis,[48–49] which is discussed in Chapter 21. In contrast to DNA, RNA can adopt a variety of three-dimensional conformations owing to its

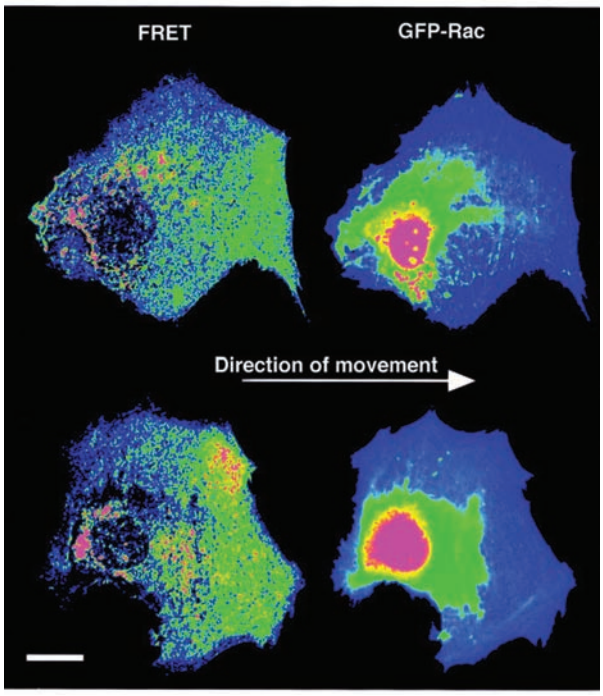

Figure 13.24. RET (left) and Rac–GFP intensity (near 510 nm) image (right) of motile 3T3 fibroblasts. Bar = 24 μm. Reprinted from [47].

single-stranded structure. Some RNA molecules are catalytically active, which are called ribozymes. RET has found use in studies of ribozyme folding and dynamics.[50–52]

Figure 13.25 shows the donor, acceptor, sequence, and secondary structure of the labeled hairpin ribozyme containing the covalently linked donor and acceptor molecules.[52] After the substrate (S) binds it is cleaved by the ribozyme. Cleavage requires binding of the A and B loops to each other, a motion called docking. This motion is expected to bring the donor and acceptor closer together (lower panel). Upon addition of substrate there are changes in both the donor and acceptor intensities (Figure 13.26). The donor intensity decreases as expected for increased energy transfer. The behavior of the acceptor is more complicated. The acceptor intensity increases as expected, but only after an initial drop in intensity on substrate binding. This decrease is due to quenching of the acceptor by the nearby guanine residue (Chapter 8).

13.6.1. Imaging of Intracellular RNA

The localization and concentration of intracellular mRNA is an important factor in the control of protein synthesis.

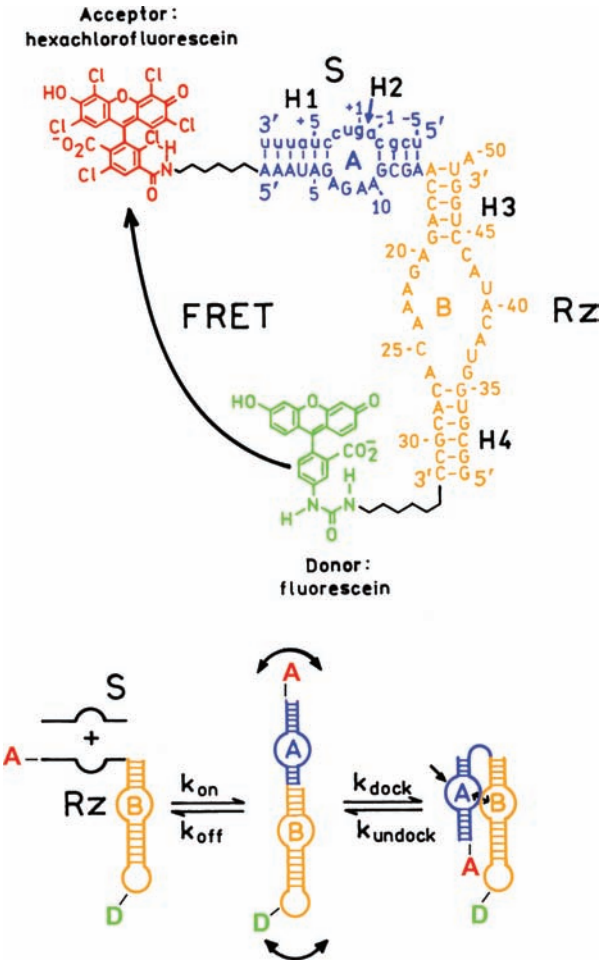

Figure 13.25. Structure of the hairpin ribozyme labeled with donor and acceptor. The lower panel shows the docking conformational change that occurs upon binding of the substrate. Revised from [52].

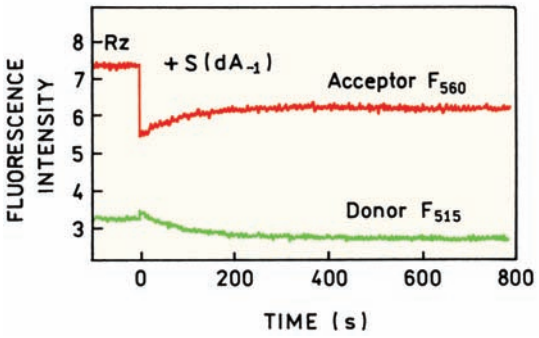

Figure 13.26. Intensity changes of the donor and acceptor on the hairpin ribozyme upon binding of substrate. Courtesy of Dr. Nils G. Walter, University of Michigan.

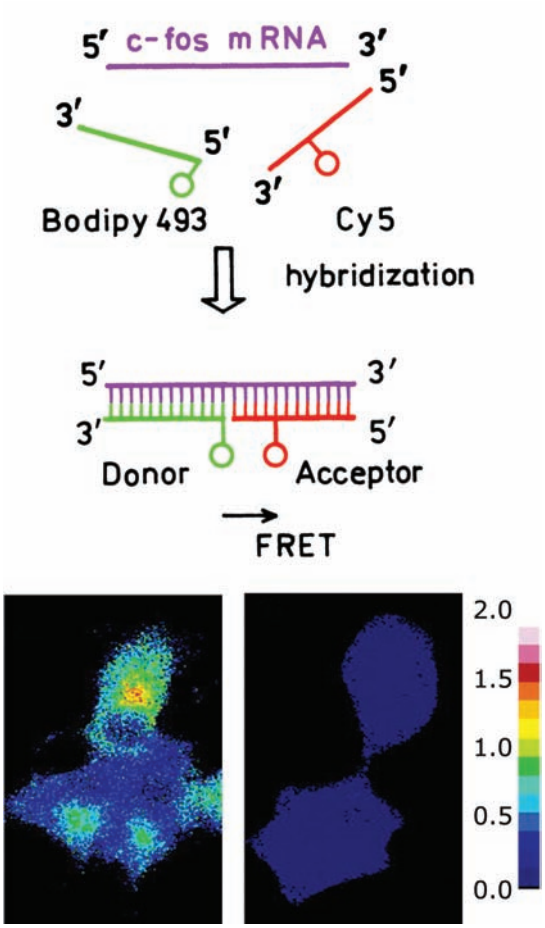

Figure 13.27. Intracellular detection of c-fos mRNA by RET ratio imaging. Revised from [53].

Control of c-fos mRNA is important because the c-fos protein is a transcription factor that participates in control of the cell cycle and differentiation. The presence of c-fos mRNA was studied using DNA oligomers that were expected to bind close to each other when hybridized with c-fos mRNA (Figure 13.27).[53] The level of c-fos mRNA could be controlled by stimulation of the Cos cells. The donor- and acceptor-labeled oligomers were added to the cells by microinjection. The presence of the mRNA was found in the stimulated (left) but not in the unstimulated cells. These results show that RET imaging can be used to study the difficult problem of the regulation of mRNA in cells.

13.7. ENERGY TRANSFER EFFICIENCY FROM ENHANCED ACCEPTOR FLUORESCENCE

In an RET experiment the acceptor absorption must overlap with the donor emission wavelengths, but the acceptor does not need to be fluorescent. If the acceptor is fluorescent then light absorbed by the donor and transferred to the acceptor appears as enhanced acceptor emission. This enhanced acceptor emission can be seen in Figure 13.16 at 520 nm for the fluorescein-labeled GroES when bound to donor-labeled GroEL. By extrapolating the emission spectrum of the donors one can see that its emission extends to the acceptor wavelengths. Hence the intensity measured at the acceptor wavelength typically contains some contribution from the donor.

The use of acceptor intensities is further complicated by the need to account for directly excited acceptor emission, which is almost always present.[13] In the case of labeled apoA-I (Figure 13.13) the directly excited acceptor emission accounted for about half the total acceptor emission. The acceptor is almost always excited directly to some extent because the acceptor absorbs at the excitation wavelength used to excite the donor, resulting in acceptor emission without RET.

Calculation of the transfer efficiency from the enhanced acceptor emission requires careful consideration of all the interrelated intensities. Assuming that the donor does not emit at the acceptor wavelength, the efficiency of transfer is given by

$$E = \frac{\varepsilon_A(\lambda_D^{ex})}{\varepsilon_D(\lambda_D^{ex})}\left[\frac{F_{AD}(\lambda_A^{em})}{F_A(\lambda_A^{em})} - 1\right]\left(\frac{1}{f_D}\right) \qquad (13.25)$$

In this expression $\varepsilon_A(\lambda_D^{ex})$ and $\varepsilon_D(\lambda_D^{ex})$ are the extinction coefficients (single D–A pairs) or absorbance (multiple acceptors) of the acceptor and donor at the donor excitation wavelength (λ_D^{ex}), and f_D is the fractional labeling with the donor. The acceptor intensities are measured at an acceptor emission wavelength (λ_A^{em}) in the absence $F_A(\lambda_A^{em})$ and presence $F_{AD}(\lambda_A^{em})$ of donor. This expression with $f_D = 1.0$ can be readily obtained by noting that $F_A(\lambda_A^{em})$ is proportional to $\varepsilon_A(\lambda_D^{ex})$, and $F_{AD}(\lambda_A^{em})$ is proportional to $\varepsilon_A(\lambda_D^{ex}) + E\varepsilon_D(\lambda_D^{ex})$. The accuracy of the measured E value is typically less than when using the donor emission (eq. 13.13). When measuring the acceptor emission it is important to have complete donor labeling, $f_D = 1.0$.

It is also important to remember that it may be necessary to correct further for the donor emission at λ_A^{em}, which is not considered in eq. 13.25. The presence of donor emission at the acceptor wavelength, if not corrected for in measuring the acceptor intensities, will result in an apparent transfer efficiency larger than the actual value (see Problem 13.11). Equation 13.25 can also be applied when mul-

tiple acceptors are present, such as for unlinked donor and acceptor pairs (Chapter 15). In this case $\varepsilon_D(\lambda_D^{ex})$ and $\varepsilon_A(\lambda_D^{ex})$ are replaced by the optical densities of the donor, $OD_D(\lambda_D^{ex})$, and of the acceptor, $OD_A(\lambda_D^{ex})$, at the donor excitation wavelength.

Occasionally it is difficult to obtain the transfer efficiency from the sensitized acceptor emission. One difficulty is a precise comparison of the donor-alone and donor–acceptor pair at precisely the same concentration. The need for two samples at the same concentration can be avoided if the donor and acceptor-labeled sample can be enzymatically digested so as to eliminate energy transfer.[54] Additionally, methods have been developed which allow comparison of the donor-alone and donor–acceptor spectra without requiring the concentrations to be the same. This is accomplished using the shape of the donor emission and subtracting its contribution from the emission spectrum of the D–A pair. This method is best understood by reading the original descriptions.[55–56]

And, finally, one should be aware of the possibility that the presence of the acceptor affects the donor fluorescence by a mechanism other than RET. Such effects could occur due to allosteric interactions between the donor and acceptor sites. For example, the acceptor may block diffusion of a quencher to the donor, or it may cause a shift in protein conformation that exposes the donor to solvent. If binding of the acceptor results in quenching of the donor by some other mechanism, then the transfer efficiency determined from the donor will be larger than the true value. In such cases, the transfer efficiency determined from enhanced acceptor emission is thought to be the correct value. The possibility of non-RET donor quenching can be addressed by comparison of the transfer efficiencies observed from donor quenching and acceptor sensitization.[57] See Problem 13.11.

13.8. ENERGY TRANSFER IN MEMBRANES

In the examples of resonance energy transfer described above there was a single acceptor attached to each donor molecule. The situation becomes more complex for unlinked donors and acceptors.[5] In this case the bulk concentration of acceptors is important because the acceptor concentration determines the D–A proximity. Also, one needs to consider the presence of more than a single acceptor around each donor. In spite of the complexity, RET has considerable potential for studies of lateral organization in membranes. For example, consider a membrane that contains regions that are in the liquid or solid phase. If the donor and acceptor both partition into the same region, one expects the extent of energy transfer to be increased relative to that expected for a random distribution of donors and acceptors between the phases. Conversely, if donor and acceptor partition into different phases, the extent of energy transfer will decrease relative to a random distribution, an effect that has been observed.[58] Alternatively, consider a membrane-bound protein. If acceptor-labeled lipids cluster around the protein, then the extent of energy transfer will be greater than expected for acceptor randomly dispersed in the membrane. Energy transfer to membrane-localized acceptors can be used to measure the distance of closest approach to a donor site on the protein, or the distance from the donor to the membrane surface.

RET in membranes is typically investigated by measuring the transfer efficiency as the membrane acceptor concentration is increased. Quantitative analysis of such data requires knowledge of the extent of energy transfer expected for fluorophores randomly distributed on the surface of a membrane. This is a complex problem that requires one to consider the geometric form of the bilayer (planar or spherical) and transfer between donors and acceptors which are on the same side of the bilayer as well as those on opposite sides. A variety of approaches have been used[58–68] and in general, numerical simulations and/or computer analyses are necessary. These theories are complex and not easily summarized. The complexity of the problem is illustrated by the fact that an analytical expression for the donor intensity for energy transfer in two dimensions only appeared in 1964,[69] and was extended to allow an excluded volume around the donor in 1979.[59] RET to multiple acceptors in one, two, and three dimensions is described in more detail in Chapter 15. Several of these results are present here to illustrate the general form of the expected data.

A general description of energy transfer on a two-dimensional surface has been given by Fung and Stryer.[5] Assuming no homotransfer between the donors, and no diffusion during the donor excited-state lifetime, the intensity decay of the donor is given by

$$I_D(t) = I_D^0 \exp(-t/\tau_D) \exp\left[-\sigma S(t)\right] \qquad (13.26)$$

where

$$S(t) = \int_{r_c}^{\infty} \{1 - \exp\left[-(t/\tau_D)(R_0/r)^6\right]\} 2\pi r\, dr \qquad (13.27)$$

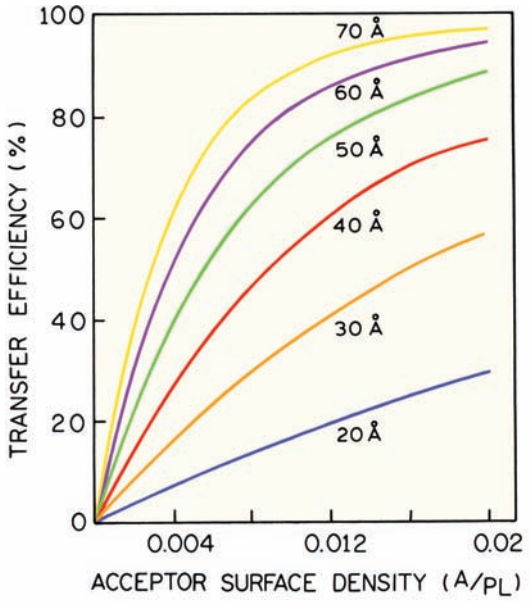

Figure 13.28. Calculated efficiencies of energy transfer for donor–acceptor pairs localized in a membrane. The distances are the R_0 value for energy transfer and A/PL is the acceptor-to-phospholipid molar ratio. The area per phospholipid was assumed to be 70 Å^2, so the distance of closest approach was 8.4 Å. Revised and reprinted with permission from [5]. Copyright © 1978, American Chemical Society.

In these equations $\exp[-\sigma S(t)]$ describes that portion of the donor decay due to RET, σ is the surface density of the acceptor, and r_c is the distance of closest approach between the donor and acceptors. The energy-transfer efficiency can be calculated by an equation analogous to eqs. 13.13 and 13.14, except that the intensities or lifetimes are calculated from integrals of the donor intensity decay:

$$E = 1 - \frac{1}{\tau_D}\int \frac{I_D(t)}{I_D^0}dt \qquad (13.28)$$

Use of eqs. 13.26–13.28 is moderately complex and requires use of numerical integration. However, the approach is quite general, and can be applied to a wide variety of circumstances by using different expressions for $S(t)$ that correspond to different geometric conditions. Figure 13.28 shows the calculated transfer efficiencies for a case in which the donor to acceptors are constrained to the lipid–water interface region of a bilayer. Several features of these predicted data are worthy of mention. The efficiency of transfer increases with R_0 and the efficiency of energy transfer is independent of the concentration of donor. The absence of energy transfer between donors is generally a safe assumption unless the donor displays a small Stokes shift or the donor concentration is high, conditions that favor homotransfer. Only small amounts of acceptor, 0.4 mole%, can result in easily measured quenching. For example, with R_0 = 40 Å the transfer efficiency is near 50% for just 0.8 mole% acceptor, or one acceptor per 125 phospholipid molecules.

One may readily visualize how energy quenching data could be used to determine whether the distributions of donor and acceptor were random. Using the calculated value of R_0, one compares the measured extent of donor quenching with the observed efficiency. If the measured quenching efficiency exceeds the calculated value then a preferential association of donors and acceptors within the membrane is indicated.[70] Less quenching would be observed if the donor and acceptor were localized in different regions of the membrane, or if the distance of closest approach were restricted due to steric factors. We note that these calculated values shown in Figure 13.28 are strictly true only for transfer between immobilized donor and acceptor on one side of a planar bilayer. However, this simple model is claimed to be a good approximation for a spherical bilayer.[5] For smaller values of R_0 transfer across the bilayer is not significant.

13.8.1. Lipid Distributions Around Gramicidin

Gramicidin is a linear polypeptide antibiotic containing D- and L-amino acids and four tryptophan residues. Its mode of action involves increasing the permeability of membranes to cations and protons. In membranes this peptide forms a dimer (Figure 13.29),[71] which contains a 4-Å diameter aqueous channel that allows diffusion of cations. The nonpolar amino acids are present on the outside of the helix, and thus expected to be exposed to the acyl side chain region of the membrane. Hence, gramicidin provides an ideal model to examine energy transfer from a membrane-bound protein to membrane-bound acceptors.

It was of interest to determine if membrane-bound gramicidin was surrounded by specific types of phospholipids. This question was addressed by measurement of the transfer efficiencies from the tryptophan donor to dansyl-labeled phosphatidylcholine (PC). The lipid vesicles were composed of phosphatidylcholine (PC) and phosphatidic acid (PA).[72] Emission spectra of gramicidin bound to PC–PA membranes are shown in Figure 13.30. The tryptophan emission is progressively quenched as the dansyl-PC

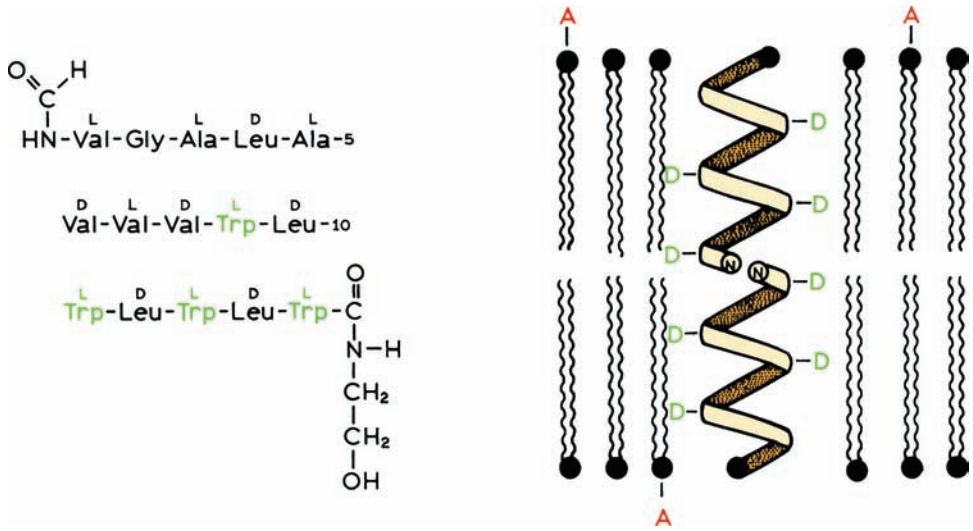

Figure 13.29. Amino-acid sequence (left) and structure of the membrane-bound dimer (right) of gramicidin A. The D and L (left) refer to the optical isomer of the amino acid. Revised from [71].

acceptor concentration is increased. The fact that the gramicidin emission is quenched by RET, rather than a collisional process, is supported by the enhanced emission of the dansyl-PC at 520 nm.

The decreasing intensities of the gramicidin emission can be used to determine the tryptophan to dansyl-PC transfer efficiencies (Figure 13.31). The transfer efficiencies are compared with the calculated efficiencies for a random acceptor distribution in two dimensions. These curves were calculated using eqs. 13.26 and 13.28. The data match with the curve calculated for the known R_0 of 24 Å, demonstrating that acceptor distribution of dansyl-PC around gramicidin is random. If the labeled lipid dansyl-PC was local-

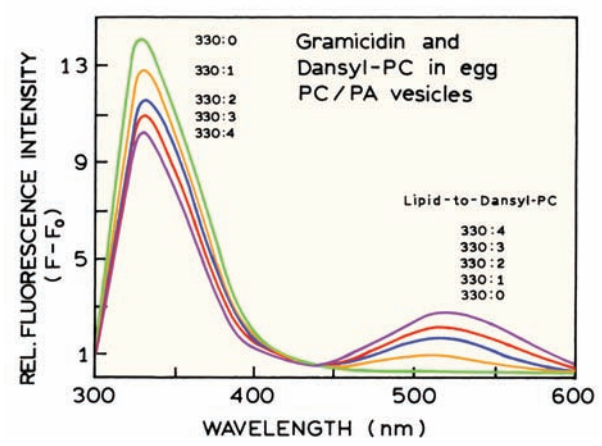

Figure 13.30. Emission spectra of gramicidin and dansyl-PC in vesicles composed of egg PC and egg PA. λ_{ex} = 282 nm. Dansyl-PC is 1-acyl-2-[11-N-[5-dimethylamino naphthalene-1-sulfonyl]amino] undecanoyl phosphatidylcholine. The lipid-to-dansyl PC ratios are shown on the figure. Revised and reprinted with permission from [72]. Copyright © 1988, American Chemical Society.

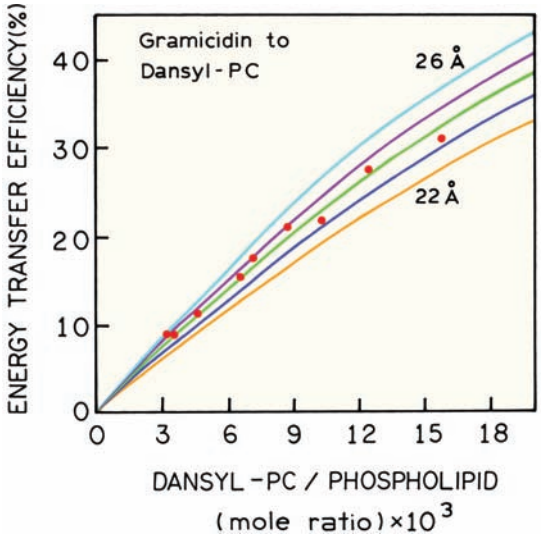

Figure 13.31. Efficiency of energy transfer from gramicidin to dansyl-PC as a function of dansyl-PC/phospholipid ratio. The experimental points (●) were calculated from the tryptophan quenching data, and the solid curves were calculated for a random array of donors and acceptors in two dimensions with R_0 = 22, 23, 24, 25, and 26 Å. A value of R_0 = 24 ± 1 Å gave the best fit to the experimental data. Revised and reprinted with permission from [72]. Copyright © 1988, American Chemical Society.

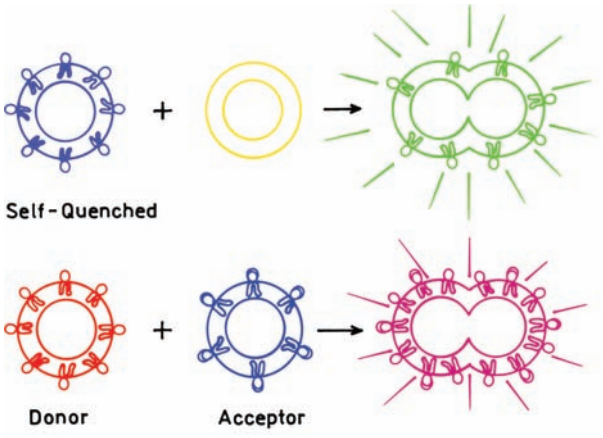

Figure 13.32. Membrane fusion detection by RET. **Top**: Homotransfer and self-quenching. Bottom: RET for a D–A pair.

ized around gramicidin then RET to the dansyl acceptor would exceed the calculated values.

13.8.2. Membrane Fusion and Lipid Exchange

Energy transfer has been widely used to study fusion and/or aggregation of membranes. These experiments are shown schematically in Figure 13.32. Suppose a lipid vesicle contains a high concentration of a fluorophore that undergoes homo-RET (Figure 13.32). Initially the membrane will be dimly fluorescent because of self-quenching (top). If this vesicle fuses with another unlabeled vesicle the extent of self-quenching will decrease and the emission intensity will increase. An alternative approach is to use RET between a donor and acceptor (bottom). In this case the vesicles labeled with each type of fluorophore will appear with different colors. Upon fusion the color will change. Depending upon the concentrations of donor and acceptor in the membranes, the extent of RET could be small, in which case the color of the fused vesicles would be a simple mixture of the two colors. If the probe concentration results in efficient RET then the fused vesicles will have the color of the acceptor.

As seen from Figure 13.28 the acceptor density does not need to be large. Any process that dilutes the donor and acceptors from the initially labeled vesicles will result in less energy transfer and increased donor emission. For example, if the D–A-labeled vesicles fuse with an unlabeled vesicle, the acceptor becomes more dilute and the donor intensity increases. Alternatively, the donor may display a modest water solubility adequate to allow exchange between vesicles. Then some of the donors will migrate to the acceptor-free vesicles and again the donor fluorescence will increase. It is also possible to trap a water-soluble fluorophore–quencher pair inside the vesicles. Upon fusion the quencher can be diluted and/or released. A wide variety of different procedures have been proposed,[73–79] but most rely on these simple proximity considerations.

RET has been used to obtain images of membranes as they fuse together. Figure 13.33 shows images of giant unilamellar vesicles (GUVs) that were labeled either with a cyanine dye DiO (left, green) or a rhodamine dye Rh–PE (right, orange).[80] The two types of vesicles contained oppositely charged lipids, which resulted in rapid fusion. The GUVs were brought together by electrophoretic migration in a fluid channel. The images were obtained with a color CCD camera, so they are real color images. Prior to contact between the GUVs, the DiO-labeled vesicle is bright and the Rh–PE-labeled vesicle dark. Rh–PE is dark because it absorbs weakly at the excitation wavelength of near 450 nm. As the vesicles make contact and fuse, a bright orange signal appears, which is due to Rh–PE. Eventually the entire vesicle surface becomes orange. The green emission from DiO is mostly quenched due to RET to Rh–PE.

13.9. EFFECT OF κ^2 ON RET

While the effect of κ^2 in energy transfer is frequently discussed,[81–82] there are relatively few experimental results.[83–86] Most of the experimental results are measurements with a single κ^2 value, rather than a systematic dependence of $k_T(r)$ or κ^2. However, the experimental results show that the value of κ^2 does affect the rate of energy transfer. Figure 13.34 shows the chemical structure of two donor–acceptor pairs. The anthracene donor was linked either in plane with the porphyrin acceptor ($\kappa^2 = 4$) or in the axial position ($\kappa^2 = 0$) The transition moment of the anthracene is along the short axis of the molecule. Emission spectra of these D–A pairs were compared to a donor control molecule. For the axial anthracene ($\kappa^2 = 0$) there is almost no RET to the porphyrin. For the in-plane anthracene with $\kappa^2 = 4$ there is almost no emission showing RET is rapid for these colinear transitions. These results show that orientation can have a dramatic effect on the RET efficiency. However, these D–A pairs are rather rigidly linked and a smaller effect is expected if the acceptor had more mobility relative to the porphyrin ring.

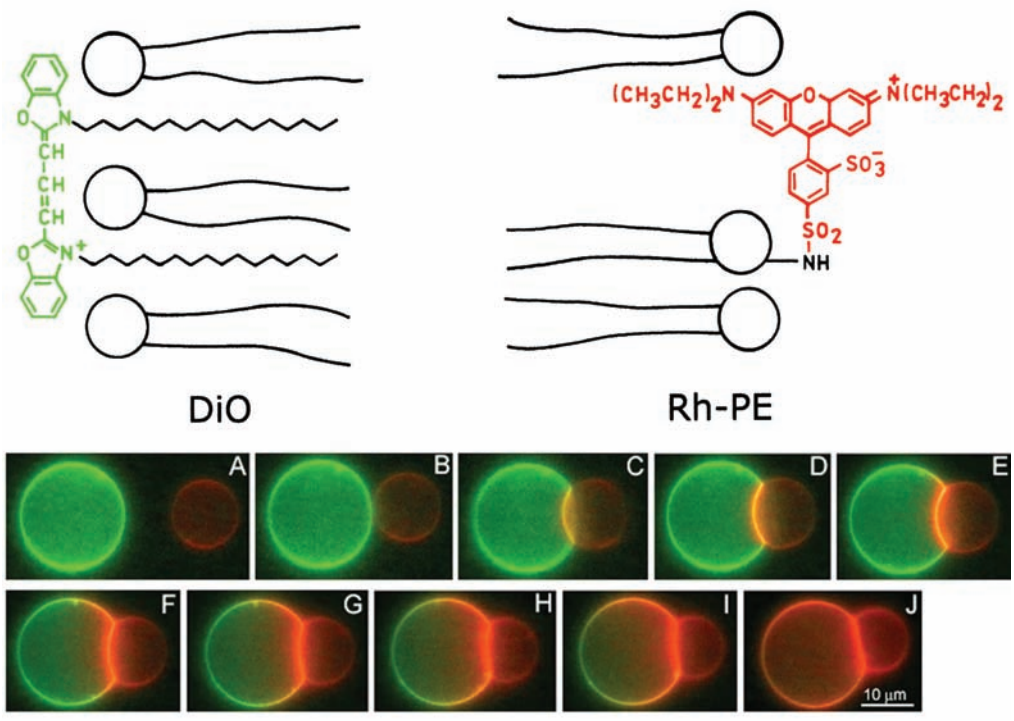

Figure 13.33. Fluorescence microscopy of lipid mixing between giant unilamellar vesicles. Reprinted from [80] and courtesy of Dr. Robert MacDonald, Northwestern University.

13.10. ENERGY TRANSFER IN SOLUTION

Energy transfer also occurs for donors and acceptors randomly distributed in three dimensional solutions. In this case the theory is relatively simple. Following δ-function excitation the intensity decay of the donor is given by[88–90]

$$I_D(t) = I_D^0 \exp\left[-t/\tau_D - 2\gamma\left(\frac{t}{\tau_D}\right)^{1/2}\right] \qquad (13.29)$$

with $\gamma = A/A_0$, where A is the acceptor concentration. If R_0 is expressed in cm, the value of A_0 in moles/liter is given by

$$A_0 = \frac{3000}{2\pi^{3/2} N R_0^3} \qquad (13.30)$$

The relative steady-state quantum yield of the donor is given by

$$\frac{F_{DA}}{F_D} = 1 - \sqrt{\pi}\,\gamma \exp(\gamma^2)\left[1 - \mathrm{erf}(\gamma)\right] \qquad (13.31)$$

where

$$\mathrm{erf}(\gamma) = \frac{2}{\sqrt{\pi}} \int_0^\gamma \exp(-x^2)\, dx \qquad (13.32)$$

These expressions are valid for immobile donors and acceptors for which the orientation factor is randomized by rotational diffusion, $\kappa^2 = 2/3$. For randomly distributed acceptors,[3] where rotation is much slower than the donor decay, $\kappa^2 = 0.476$. Still more complex expressions are necessary if the donor and acceptor diffuse during the lifetime of the excited state (Chapters 14 and 15). The complex decay of donor fluorescence reflects the time-dependent population of D–A pairs. Those donors with nearby acceptors decay more rapidly, and donors more distant from acceptors decay more slowly.

The term A_0 is called the critical concentration and represents the acceptor concentration that results in 76% energy transfer. This concentration in moles/liter (M) can be calculated from eq. 13.30, or from a simplified expression[14]

$$A_0 = 447/R_0^3 \qquad (13.33)$$

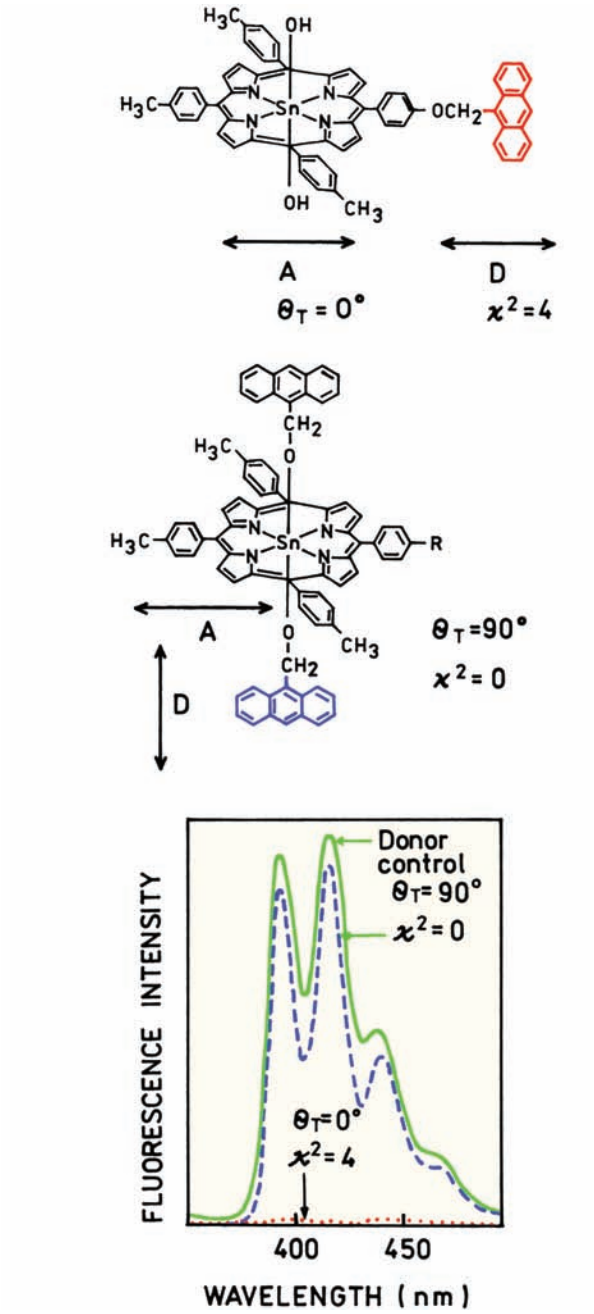

Figure 13.34. Chemical structures and emission spectra of covalently linked D–A pairs used to study the effect of κ^2 on RET. Revised from [87].

where R_0 is in units of Å. This reveals an important feature of energy transfer between unlinked donors and acceptors, which is that the acceptor concentrations need to be rather high for RET between unlinked donor and acceptors. For instance, if $R_0 = 25$ Å, then $A_0 = 0.029$ M = 29 mM. Because A_0 is orders of magnitude larger than typical concentrations in fluorescence experiments, we usually ignore energy transfer between donors and acceptors linked to different molecules. The high acceptor concentrations needed for RET in solution also make it difficult to measure RET between unlinked donors and acceptors. The high acceptor concentrations result in high optical densities, requiring front face observation and careful correction for inner filter effects. It is important to consider inner filter effects when comparing intensity values.

13.10.1. Diffusion-Enhanced Energy Transfer

To this point we have not considered the effects of diffusion on the extent of energy transfer. This is a complex topic that typically requires numerical methods for simulations and analysis of the data. However, there is one simple case in which the donor decay times are very long so that diffusive motions of the donors result in their sampling of the entire available space. This is called the rapid diffusion limit.[91] With fluorophores displaying ns decay times this limit is not obtainable. However, lanthanides are known to display much longer decay times near 0.6–2.5 ms for terbium and europium,[92–93] depending upon the ligands. In relatively fluid solution the long donor decay times allow the excited molecule to diffuse through all available space. The rate of transfer then becomes limited by the distance of closest approach between donors and acceptors. Suppose an acceptor is buried in a protein or a membrane. One can determine the depth of the acceptor from the extent of energy transfer to the acceptor from terbium or europium chelates in the aqueous phase. Another important feature of energy transfer in the rapid-diffusion limit is that it occurs at much lower acceptor concentrations.[91] For a homogeneous three-dimensional solution, energy transfer is 50% efficient at acceptor concentrations near 1 μM, which is 1000-fold lower than for energy transfer without diffusion.[14] This topic is described in detail in Chapter 15.

13.11. REPRESENTATIVE R_0 VALUES

It is often convenient to have an estimate of an R_0 value prior to performing the complex calculation of the overlap integral or labeling of the macromolecule. Unfortunately, there is no general reference for the Förster distances. A larger number of R_0 values are summarized in the book by Berlman,[94] but most of the listed fluorophores are not used in biochemistry. A large number of Förster distances have been summarize in reviews.[14,95] Some of these R_0 values are

Table 13.3. Representative Förster Distances for Various Donor–Acceptor Pairs[a]

Donor	Acceptor	R_0 (Å)
Naphthalene[14]	Dansyl	22
Dansyl[95]	FITC	33–41
Dansyl[14]	ODR	43
ε-A[14]	NBD	38
IAF[14]	TMR	37–50
Pyrene[14]	Coumarin	39
FITC[14]	TMR	49–54
IAEDANS[14]	FITC	49
IAEDANS[14]	IAF	46–56
IAF[14]	EIA	46
CF	TR	51
Bodipy[25]	Bodipy	57
BPE[14]	Cy5	72
Terbium[96]	Rhodamine	65
Europium[94]	Cy5	70
Europium[97]	APC	90

[a]Dansyl, 5-dimethylamino-1-napthalenesulfonic acid. ε-A, 1-N[6]-ethenoadenosine; APC, allophycocyanin; Bodipy, 4,4-difluoro-4-bora-3a,4a-diaza-s-indacene; BPE, B-phycoerythrin; CF, carboxylfluorescein, succinimidyl ester; Cy5, carboxymethylindocyanine-N-hydroxysuccinimidyl ester; EIA, 5-(iodoacetamido) eosin; FITC, fluorescein-5-isothiocyanate; IAEDANS, 5-(2-0((iodocetyl)amino)ethyl)amino)naphthalene-1-sulfonic acid; IAF, 5-iodoacetamidofluorescein; NBD, 7-nitrobenz-2-oxa-1,3-diazol-4-yl; ODR, octadecylrhodamine; TMR, tetramethylrhodamine; TR, Texas Red.

Table 13.4. Förster Distances for Tryptophan–Acceptor Pairs[a]

Donor	Acceptor[b]	R_0 (Å)
Trp	Nitrobenzoyl	16
Trp	Dansyl	21–24
Trp	IAEDANS	22
Trp	Anthroyloxyl	24
Trp	TNB	24
Trp	Anthroyl	25
Trp	Tyr–NO_2	26
Trp	Pyrene	28
Trp	Heme	29
Trp	NBS	30
Trp	DNBS	33
Trp	DPH	40

[a]From [14].

[b]ANS, 6-anilinonaphthalene-2-sulfonic acid; Dansyl, 5-dimethylamino-1-napthalenesulfonic acid; DPH, 1,6-diphenyl-1,3,5-hexatriene; DNBS, dinitrobenzenesulfonyl; IAEDANS, 5-(((2-iodocetyl)amino)ethyl)amino)-naphthalene-1-sulfonic acid; NBS, nitrobenzenesulfenyl; TNB, trinitrophenyl; TNB, trinitrophanyl.

summarized in Table 13.3 for a variety of D–A pairs, and in Table 13.4 for tryptophan donor–acceptor pairs. In the case of lanthanides in environments where the quantum yield is near unity, and for multi-chromophore acceptors, R_0 values as large as 90 Å have been calculated.[95] This is the largest Förster distance reported to date.

REFERENCES

1. Förster Th. 1948. Intermolecular energy migration and fluorescence. *Ann Phys* 2:55–75. [Translated by RS Knox, Department of Physics and Astronomy, University of Rochester, Rochester, NY 14627.]
2. Stryer L. 1978. Fluorescence energy transfer as a spectroscopic ruler. *Annu Rev Biochem* **47**:819–846.
3. Steinberg IZ. 1971. Long-range nonradiative transfer of electronic excitation energy in proteins and polypeptides. *Annu Rev Biochem* **40**:83–114.
4. Clegg RM. 1996. Fluorescence resonance energy transfer. In *Fluorescence imaging spectroscopy and microscopy*, pp. 179–252. Ed XF Wang, B Herman. John Wiley & Sons, New York.
5. Fung BKK, Stryer L. 1978. Surface density determination in membranes by fluorescence energy transfer. *Biochemistry* **17**:5241–5248.
6. Yekta A, Duhamel J, Winnik MA. 1995. Dipole–dipole electronic energy transfer: fluorescence decay functions for arbitrary distributions of donors and acceptors—systems with planar geometry. *Chem Phys Lett* **235**:119–125.
7. Rolinski OJ, Birch DJS. 2000. Determination of acceptor distribution from fluorescence resonance energy transfer: theory and simulation. *J Chem Phys* **112**(20):8923–8933.
8. Weller A. 1974. Theodor Förster. *Ber Bunsenges Phys Chem* **78**:969–971.
9. Gordon M, Ware WR., eds. 1975. *The exciplex*. Academic Press, New York. [See the Introduction about Theodor Förster.]
10. Dale RE, Eisinger J, Blumberg WE. 1979. The orientational freedom of molecular probes: the orientation factor in intramolecular energy transfer. *Biophys J* **26**:161–194; *Errata* **30**:365 (1980).
11. Dale RE, Eisinger J. 1975. Polarized excitation energy transfer. In *Biochemical fluorescence, concepts*, Vol. 1, pp. 115–284. Ed RF Chen, H Edelhoch. Marcel Dekker, New York.
12. Dale RE, Eisinger J. 1974. Intramolecular distances determined by energy transfer: dependence on orientational freedom of donor and acceptor. *Biopolymers* **13**:1573–1605.
13. Cheung HC. 1991. Resonance energy transfer. In *Topics in fluorescence spectroscopy*, Vol. 2: *Principles*, pp. 127–176. Ed JR Lakowicz. Plenum Press, New York.
14. Wu P, Brand L. 1994. Resonance energy transfer: methods and applications [review]. *Anal Biochem* **218**:1–13.
15. Dos Remedios CG, Moens PDJ. 1995. Fluorescence resonance energy transfer spectroscopy is a reliable "ruler" for measuring structural changes in proteins. *J Struct Biol* **115**:175–185.

16. Haas E, Katchalski-Katzir E, Steinberg IZ. 1978. Effect of the orientation of donor and acceptor on the probability of energy transfer involving electronic transitions of mixed polarizations. *Biochemistry* **17**:5064–5070.
17. Latt SA, Cheung HC, Blout ER. 1965. Energy transfer: a system with relatively fixed donor-acceptor separation. *J Am Chem Soc* **87**(5): 996–1003.
18. Stryer L, Haugland RP. 1967. Energy transfer: a spectroscopic ruler. *Proc Natl Acad Sci USA* **58**:719–726.
19. Gabor G. 1968. Radiationless energy transfer through a polypeptide chain. *Biopolymers* **6**:809–816.
20. Haugland RP, Yguerabide J, Stryer L. 1969. Dependence of the kinetics of singlet-singlet energy transfer on spectral overlap. *Proc Natl Acad Sci USA* **63**:23–30.
21. Horrocks WDeW, Holmquist B, Vallee BL. 1975. Energy transfer between terbium(III) and cobalt(II) in thermolysin: a new class of metal–metal distance probes. *Proc Natl Acad Sci USA* **72**(12): 4764–4768.
22. Xiao M, Selvin PR. 2001. Quantum yields of luminescent lanthanide chelates and far-red dyes measured by resonance energy transfer. *J Am Chem Soc* **123**:7067–7073.
23. Chen J, Selvin PR. 2000. Lifetime- and color-tailored fluorophores in the micro- to millisecond time regime. *J Am Chem Soc* **122**: 657–660.
24. BODIPY, 4,4-difluoro-4-bora-3a,4a-diaza-s-indacene. BODIPY is a trademark of Molecular Probes Inc.
25. Johnson ID, Kang HC, Haugland RP. 1991. Fluorescent membrane probes incorporating dipyrrometheneboron difluoride fluorophores. *Anal Biochem* **198**:228–237.
26. Hemmila IA, ed. 1991. *Applications of fluorescence in immunoassays*. John Wiley & Sons, New York (see p. 113).
27. Malicka J, Gryczynski I, Lakowicz JR, 2003. Enhanced emission of highly labeled DNA oligomers near silver metallic surfaces. *Anal Chem* **75**:4408–4414.
28. Lakowicz JR, Malicka J, D'Auria S, Gryczynski I. 2003. Release of the self-quenching of fluorescence near silver metallic surfaces. *Anal Biochem* **320**:13–20.
29. Kawski A. 1983. Excitation energy transfer and its manifestation in isotropic media. *Photochem Photobiol* **38**(4):487–504.
30. Song X, Swanson BI. 2001. Rapid assay for avidin and biotin based on fluorescence quenching. *Anal Chim Acta* **442**:79–87.
31. Lakowicz JR, Gryczynski I, Wiczk W, Laczko G, Prendergast FC, Johnson ML. 1990. Conformational distributions of melittin in water/methanol mixtures from frequency-domain measurements of nonradiative energy transfer. *Biophys Chem* **36**:99–115.
32. Faucon JF, Dufourca J, Lurson C. 1979. The self-association of melittin and its binding to lipids. *FEBS Lett* **102**:187–190.
33. Goto Y, Hagihara Y. 1992. Mechanism of the conformational transition of melittin. *Biochemistry* **31**:732–738.
34. Cheung HC, Gonsoulin F, Garland F. 1983. Fluorescence energy transfer studies on the proximity of the two essential thiols of myosin subfragment-1. *J Biol Chem* **258**(9):5775–5786.
35. Lakowicz JR, Gryczynski I, Cheung HC, Wang C-K, Johnson ML, Joshi N. 1988. Distance distributions in proteins recovered by using frequency-domain fluorometry: applications to Troponin I and its complex with Troponin C. *Biochemistry* **27**:9149–9160.
36. Li HH, Lyles DS, Thomas MJ, Pan W, Sorci-Thomas MG. 2000. Structural determination of lipid-bound ApoA-I using fluorescence resonance energy transfer. *J Biol Chem* **275**(47):37048–37054.
37. Tricerri MA, Agree AKB, Sanchez SA, Bronski J, Jonas A. 2001. Arrangement of apolipoprotein A-I in reconstituted high-density lipoprotein disks: an alternative model based on fluorescence resonance energy transfer experiments. *Biochemistry* **40**:5065–5074.
38. Xu Q, Brecht WJ, Weisgraber KH, Mahley RW, Huang Y. 2004. Apolipoprotein E4 domain interaction occurs in living neuronal cells as determined by fluorescence resonance energy transfer. *J Biol Chem* **279**(24):25511–25516.
39. Berney C, Danuser G. 2003. FRET or no FRET: a quantitative comparision. *Biophys J* 84:3992–4010.
40. Hoppe A, Christensen K, Swanson JA. 2002. Fluorescence resonance energy transfer-based stoichiometry in living cells. *Biophys J* **83**:3652–3664.
41. Gordon GW, Berry G, Liang XH, Levine B, Herman B. 1998. Quantitative fluorescence resonance energy transfer measurements using fluorescence microscopy. *Biophys J* **74**:2702–2713.
42. Rye HS. 2001. Application of fluorescence resonance energy transfer to the GroEL–GroES chaperonin reaction. *Methods* **24**:278–288.
43. Chapman ER, Alexander K, Vorherr T, Carafoli E, Storm DR. 1992. Fluorescence energy transfer analysis of calmodulin–peptide complexes. *Biochemistry* **31**:12819–12825.
44. Medintz IL, Konnert JH, Clapp AR, Stanish I, Twigg ME, Mattoussi H, Mauro JM, Deschamps JR. 2004. A fluorescence resonance energy transfer-derived structure of a quantum dot-protein bioconjugate nanoassembly. *Proc Natl Acad Sci USA* **101**(26):9612–9617.
45. Awais M, Sato M, Sasaki K, Umezawa Y. 2004. A genetically encoded fluorescent indicator capable of discriminating estrogen agonists from antagonists in living cells. *Anal Chem* **76**:2181–2186.
46. Sato M, Ozawa T, Inukai K, Asano T, Umezawa Y. 2002. Fluorescent indicators for imaging protein phosphorylation in single living cells. *Nature Biotechnol* **20**:287–294.
47. Kraynov VS, Chamberlain C, Bokoch GM, Schwartz MA, Slabaugh S, Hahn KM. 2000. Localized Rac activation dynamics visualized in living cells. *Science* **290**:333–337.
48. Parkhurst KM, Parkhurst LJ. 1996. Detection of point mutations in DNA by fluorescence energy transfer. *J Biomed Opt* **1**(4):435–441.
49. Morrison LE, Stols LM. 1993. Use of FRET to measure association of DNA oligomers. *Biochemistry* **32**:3095–3104.
50. Bassi GS, Murchie AIH, Walter F, Clegg RM, Lilley DMJ. 1997. Ion-induced folding of the hammerhead ribozyme: a fluorescence resonance energy transfer study. *EMBO J* **16**(24):7481–7489.
51. Walter NG. 2001. Structural dynamics of catalytic RNA highlighted by fluorescence resonance energy transfer. *Methods* **25**:19–30.
52. Walter NG, Hampel KJ, Brown KM, Burke JM. 1998. Tertiary structure formation in the hairpin ribozyme monitored by fluorescence resonance energy transfer. *EMBO J* **17**(8):2378–2391.
53. Tsuji A, Koshimoto H, Sato Y, Hirano M, Sei-Iida Y, Kondo S, Ishibashi K. 2000. Direct observation of specific messenger RNA in a single living cell under a fluorescence microscope. *Biophys J* **78**:3260–3274.
54. Epe B, Steinhauser KG, Woolley P. 1983. Theory of measurement of Förster-type energy transfer in macromolecules. *Proc Natl Acad Sci USA* **80**:2579–2583.

55. Clegg RM. 1992. Fluorescence resonance energy transfer and nucleic acids. *Methods Enzymol* **211**:353–388.
56. Clegg RM, Murchie AIH, Lilley DM. 1994. The solution structure of the four-way DNA junction at low-salt conditions: a fluorescence resonance energy transfer analysis. *Biophys J* **66**:99–109.
57. Berman HA, Yguerabide J, Taylor P. 1980. Fluorescence energy transfer on acetylcholinesterase: spatial relationships between peripheral site and active center. *Biochemistry* **19**:2226–2235.
58. Pedersen S, Jorgensen K, Baekmark TR, Mouritsen OG. 1996. Indirect evidence for lipid-domain formation in the transition region of phospholipid bilayers by two-probe fluorescence energy transfer. *Biophys J* **71**:554–560.
59. Estep TN, Thomson TE. 1979. Energy transfer in lipid bilayers. *Biophys J* **26**:195–207.
60. Wolber PK, Hudson BS. 1979. An analytical solution to the Förster energy transfer problem in two dimensions. *Biophys J* **28**:197–210.
61. Dewey TG, Hammes GG. 1980. Calculation of fluorescence resonance energy transfer on surfaces. *Biophys J* **32**:1023–1035.
62. Shaklai N, Yguerabide J, Ranney HM. 1977. Interaction of hemoglobin with red blood cell membranes as shown by a fluorescent chromophore. *Biochemistry* **16**:5585–5592.
63. Snyder B, Freire E. 1982. Fluorescence energy transfer in two dimensions. *Biophys J* **40**:137–148.
64. Yguerabide J. 1994. Theory for establishing proximity relations in biological membranes by excitation energy transfer measurements. *Biophys J* **66**:683–693.
65. Dewey TG. 1991. Fluorescence energy transfer in membrane biochemistry. In *Biophysical and biochemical aspects of fluorescence spectroscopy*, pp. 294–315. Ed TG Dewey. Plenum Press, New York.
66. Dobretsov GE, Kurek NK, Machov VN, Syrejshehikova TI, Yakimenko MN. 1989. Determination of fluorescent probes localization in membranes by nonradiative energy transfer. *J Biochem Biophys Meth* **19**:259–274.
67. Yekta A, Duhamel J, Winnik MA. 1995. Dipole–dipole electronic energy transfer: fluorescence decay functions for arbitrary distributions of donors and acceptors—systems with planar geometry. *Chem Phys Lett* **235**:119–125.
68. Tcherkasskaya O, Klushin L, Gronenborn AM. 2002. Effective lattice behavior of fluorescence energy transfer at lamellar macromolecular interfaces. *Biophys J* **82**:988–995.
69. Tweet AG, Bellamy WD, Gaines GL. 1964. Fluorescence quenching and energy transfer in monomolecular films containing chlorophyll. *J Chem Phys* **41**(1):2068–2077.
70. Loura LMS, Fedorov A, Prieto M. 1996. Resonance energy transfer in a model system of membranes: application to gel and liquid crystalline phases. *Biophs J* **71**:1823–1836.
71. Stryer L, ed. 1995. *Biochemistry*, 4th ed. W.H. Freeman, New York [see p. 274].
72. Wang S, Martin E, Cimino J, Omann G, Glaser M. 1988. Distribution of phospholipids around gramicidin and D-â-hydroxybutyrate dehydrogenase as measured by resonance energy transfer. *Biochemistry* **27**:2033–2039.
73. Ladokhin AS, Wimley WC, Hristova K, White SH. 1997. Mechanism of leakage of contents of membrane vesicles determined by fluorescence requenching. *Methods Enzymol* **278**:474–486.
74. Kok JW, Hoekstra D. 1993. Fluorescent lipid analogues applications in cell and membrane biology. In *Biological techniques: fluorescent and luminescent probes for biological activity*, pp. 101–119. Ed WT Mason. Academic Press, New York.
75. Pyror C, Bridge M, Loew LM. 1985. Aggregation, lipid exchange, and metastable phases of dimyristoylphosphatidylethanolamine vesicles. *Biochemistry* **24**:2203–2209.
76. Duzgunes N, Bentz J. 1988. Use of membrane-associated fluorescence probes to monitor fusion of bilayer vesicles. In *Spectroscopic membrane probes*, pp. 117–159. Ed LD Loew. CRC Press, Boca Raton, FL.
77. Silvius JR, Zuckermann MJ. 1993. Interbilayer transfer of phospholipid-anchored macromolecules via monomer diffusion. *Biochemistry* **32**:3153–3161.
78. El Jastimi R, Lafleur M. 1999. A dual-probe fluorescence method to examine selective perturbations of membrane permeability by melittin. *Biospectroscopy* **5**:133–140.
79. Malinin VS, Haque ME, Lentz BR. 2001. The rate of lipid transfer during fusion depends on the structure of fluorescent lipid probes: a new chain-labeled lipid transfer probe pair. *Biochemistry* **40**:8292–8299.
80. Lei G, MacDonald RC. 2003. Lipid bilayer vesicle fusion: intermediates captured by high-speed microfluorescence spectroscopy. *Biophys J* **85**:1585–1599.
81. Srinivas G, Bagchi B. 2001. Effect of orientational motion of mobile chromophores on the dynamics of Förster energy transfer in polymers. *J Phys Chem B* **105**:9370–9374.
82. Artyukhov VY, Mayer GV. 2001. Theoretical study of the effect of orientation and solvent on energy transfer on bichromophore systems. *Mol Spectrosc* **90**(5):664–668.
83. Ronova IA, Kovalevsky AY, Siling SA, Shamshin SV, Grachev AV, Tsyganova OY. 2001. Bifluorophores: molecular design and excitation energy transfer mechanism. *Chem Phys* **270**:99–108.
84. Zhong D, Pal SK, Zhang D, Chan SI, Zewail AH. 2002. Femtosecond dynamics of rubredoxin: tryptophan solvation and resonance energy transfer in the protein. *Proc Natl Acad Sci USA* **99**(1):13–18.
85. Wong KF, Bagchi B, Rossky PJ. 2004. Distance and orientation dependence of excitation transfer rates in conjugated systems: beyond the Förster theory. *J Phys Chem A* **108**:5752–5763.
86. Toniolo C, Formaggio F, Crisma M, Mazaleyrat JP, Wakselman GC, Deschamps JR, Flippen-Anderson JL, Pispisa B, Venanzi M, Palleschi A. 1999. First peptide-based system of rigid donor–rigid interchromophore spacer–rigid acceptor: a structural and photophysical study. *Chem-Eur J* **5**(8):2254–2264.
87. Giribabu L, Kumar AA, Neeraja V, Maiya BG. 2001. Orientation dependence of energy transfer in an anthracene–porphyrin donor–acceptor system. *Angew Chem Int Ed* **40**(19):3621–3624.
88. Bennett RG. 1964. Radiationless intermolecular energy transfer, I: singlet–singlet transfer. *J Chem Phys* **41**:3037–3041.
89. Eisenthal KB, Siegel S. 1964. Influence of resonance transfer on luminescence decay. *J Chem Phys* **41**:652–655.
90. Birks JB, Georghiou S. 1968. Energy transfer in organic systems, VII: effect of diffusion on fluorescence decay. *Proc Roy Soc (J Phys B)* **1**:958–965.
91. Thomas DD, Caslsen WF, Stryer L. 1978. Fluorescence energy transfer in the rapid diffusion limit. *Proc Natl Acad Sci USA* **75**:5746–5750.
92. Selvin PR, Rana TM, Hearst JE. 1994. Luminescence resonance energy transfer. *J Am Chem Soc* **116**:6029–6030.

93. Li M, Selvin PR. 1995. Luminescent polyaminocarboxylate chelates of terbium and europium: the effects of chelate structure. *J Am Chem Soc* **117**:8132–8138.
94. Berlman IB. 1973. *Energy transfer parameters of aromatic compounds*. Academic Press, New York.
95. Fairclough RH, Cantor CR. 1978. The use of singlet energy transfer to study macromolecular assemblies. *Methods Enzymol* **48**:347–379.
96. Selvin PR. 1995. Fluorescence resonance energy transfer. *Methods Enzymol* **246**:300–334.
97. Mathis G. 1993. Rare earth cryptates and homogeneous fluoroimmunoassays with human sera. *Clin Chem* **39**(9):1953–1959.
98. Lakowicz JR, Johnson ML, Wiczk W, Bhat A, Steiner RF. 1987. Resolution of a distribution of distances by fluorescence energy transfer and frequency-domain fluorometry. *Chem Phys Letts* **138**(6):587–593.
99. Johnson DA, Leathers VL, Martinez AM, Walsh DA, Fletcher WH. 1993. Fluorescence resonance energy transfer within a heterochromatic cAMP-dependent protein kinase holoenzyme under equilibrium conditions: new insights into the conformational changes that result in cAMP-dependent activation. *Biochemistry* **32**:6402–6410.

ADDITIONAL REFERENCES ON RESONANCE ENERGY TRANSFER

Association Reactions

Amiri H, Schultz G, Schaefer M. 2003. FRET-based analysis of TRPC subunit stoichiometry. *Cell Calcium* **33**:463–470.
Chatterjee SK, Laffray J, Patel P, Ravindra R, Qin Y, Kuehne ME, Bane SL. 2002. Interaction of tubulin with a new fluorescent analogue of vinblastine. *Biochemistry* **41**:14010–14018.
Derdowski A, Ding L, Spearman P. 2004. A novel fluorescence resonance energy transfer assay demonstrates that the human immunodeficiency virus type 1 $Pr55^{Gag}$ I domain mediates Gag–Gag interactions. *J Virol* **78**(3):1230–1242.
Li M, Reddy LG, Bennett R, Silva ND, Jones LR, Thomas DD. 1999. A fluorescence energy transfer method for analyzing protein oligomeric structure: application to phospholamban. *Biophys J* **76**:2587–2599.

DNA

Lee BW, Moon SJ, Youn MR, Kim JH, Jang HG, Kim SK. 2003. DNA mediated resonance energy transfer from 4',6-diamidino-2-phenylindole to $[Ru(1,10\text{-phenanthroline})_2L]^{2+}$. *Biophys J* **85**:3865–3871.
Norman DG, Grainger RJ, Uhrín D, Lilley DMJ. 2000. Location of cyanine-3 on double-stranded DNA: importance for fluorescence resonance energy transfer studies. *Biochemistry* **39**:6317–6324.
Murchie AIH, Clegg RM, von Kitzing E, Duckett DR, Diekmann S, Lilley DMJ. 1989. Fluorescence energy transfer shows that the four-way DNA junction is a right-handed cross of antiparallel molecules. *Nature* **341**:763–766.
Wang L, Gaigalas AK, Blasic J, Holden MJ, Gallagher DT, Pires R. 2003. Fluorescence resonance energy transfer between donor–acceptor pai on two oligonucleotides hybridized adjacently to DNA template. *Biopolymers* **72**:401–412.

Dendrimers

Adronov A, Gilat SL, Fréchet JMJ, Ohta K, Neuwahl FVR, Fleming GR. 2000. Light harvesting and energy transfer in laser-dye-labeled poly(aryl ether) dendrimers. *J Am Chem Soc* **122**:1175–1185.
Balzani V, Ceroni P, Gestermann S, Gorka M, Kauffmann C, Maestri M, Vögtle F. 2000. Eosin molecules hosted into a dendrimer which carries thirty-two dansyl units in the periphery: a photophysical study. *Chem Phys Chem* **4**:224–227.
Brousmiche DW, Serin JM, Fréchet JMJ, He GS, Lin TC, Chung SJ, Prasad PN, Kannan R, Tan LS. 2004. Fluorescence resonance energy transfer in novel multiphoton absorbing dendritic structures. *J Phys Chem B* **108**:8592–9600.
Maus M, De R, Lor M, Weil T, Mitra S, Wiesler UM, Herrmann A, Hofkens J, Vosch T, Müllen H, De Schryver FC. 2001. Intramolecular energy hopping and energy trapping in polyphenylene dendrimers with multiple peryleneimide donor chromophores and a terryleneimide acceptor trap chromophore. *J Am Chem Soc* **123**:7668–7676.

Experimental Methods

Guptasarma P, Raman B. 1995. Use of tandem cuvettes to determine whether radiative (Trivial) energy transfer can contaminate steady-state measurements of fluorescence resonance energy transfer. *Anal Biochem* **230**:187–191.

Homo-Resonance Energy Transfer

Hamann S, Kiilgaard JF, Litman T, Alvarez-Leefmans FJ, Winther BR, Zeuthen T. 2002. Measurement of cell volume changes by fluorescence self-quenching. *J Fluoresc* **12**(2):139–145.
Kalinin S, Molotkovsky JG, Johansson LBA. 2003. Distance measurements using partial donor-donor energy migration within pairs of fluorescent groups in lipid bilayers. *J Phys Chem B* **107**:3318–3324.

Membranes

Pentcheva T, Edidin M. 2001. Clustering of peptide-loaded MHC Class I molecules for endoplasmic reticulum export imaged by fluorescence resonance energy transfer. *J Immunol* **166**:6625–6632.
Polozov IV, Polozova AI, Molotkovsky JG, Epand RM. 1997. Amphipathic peptide affects the lateral domain organization of lipid bilayers. *Biochim Biophys Acta* **1328**:125–139.

Multiple-Step RET

Galperin E, Verkhusha VV, Sorkin A. 2004. Three-chromophore FRET microscopy to analyze multiprotein interactions in living cells. *Nature Methods* **1**(3):209–217.
Ohya Y, Yabuki K, Hashimoto M, Nakajima A, Ouchi T. 2003. Multistep fluorescence resonance energy transfer in sequential chromophore array constructed on oligo-DNA assemblies. *Bioconjugate Chem* **14**(6):1057–1066.

Tong AK, Jockusch S, Li Z, Zhu HR, Akins DL, Turro NJ, Ju J. 2001. Triple fluorescence energy transfer in covalently trichromophore-labeled DNA. *J Am Chem Soc* **123**:12923–12924.

Wang S, Gaylord BS, Bazan GC. 2004. Fluorescein provides a resonance gate for FRET from conjugated polymers to DNA intercalated dyes. *J Am Chem Soc* **126**:5446–5451.

Orientation Factor

Håkansson P, Isaksson M, Westlund P-O, Johansson LB-A. 2004. Extended Förster theory for determining intraprotein distances: I: the κ^2-dynamics and fluorophore reorientation. *J Phys Chem* **108**:17243–17250.

Schartel B, Krüger S, Wachtendorf V, Hennecke M. 2000. Excitation energy transfer of a bichromophoric cross-shaped molecule investigated by polarized fluorescence spectroscopy. *J Chem Phys* **112**(22):9822–9827.

Protein Folding

Cai K, Schircht V. 1996. Structural studies on folding intermediates of serine hydroxymethyltransferase using fluorescence resonance energy transfer. *J Biol Chem* **271**(44):27311–27320.

Fisher CA, Narayanaswami V, Ryan RO. 2000. The lipid-associated conformation of the low density lipoprotein receptor binding domain of human apolipoprotein E*. *J Biol Chem* **275**(43):33601–33606.

Hammarstrom P, Persson M, Carlsson U. 2001. Protein compactness measured by fluorescence resonance energy transfer. *J Biol Chem* **276**(24):21765–21775.

Krishnakumar SS, Panda D. 2002. Spatial relationship between the prodan site, Trp-214, and Cys-34 residues in human serum albumin and loss of structure through incremental unfolding. *Biochemistry* **41**: 7443–7452.

Lakey JH, Duche D, Gonzalez-Manas JM, Baty D, Pattus F. 1993. Fluorescence energy transfer distance measurements: the hydrophobic helical hairpin of colicin A in the membrane bound state. *J Mol Biol* **230**:1055–1067.

Lillo MP, Szpikowska BK, Mas MT, Sutin JD, Beechem JM. 1997. Real-time measurement of multiple intramolecular distances during protein folding reactions: a multisite stopped-flow fluorescence energy-transfer study of yeast phosphoglycerate kinase. *Biochemistry* **36**: 11273–11281.

Protein Motions

Bilderback T, Fulmer T, Mantulin WW, Glaser M. 1996. Substrate binding causes movement in the ATP binding domain of *Escherichia coli* adenylate kinase. *Biochemistry* **35**:6100–6106.

Reviews

Chirio-Lebrun MC, Prats M. 1998. Fluorescence resonance energy transfer (FRET): theory and experiments. *Biochem Educ* **26**:320–323.

Clegg RM, 2004. Nuts and bolts of excitation energy migration and energy transfer. In *Chlorophyll fluorescence: a signature of photosynthesis*. Ed GC Papageorgiou, Govindjee. Kluwer, Dordrecht.

Clegg RM. 2004. The vital contributions of Perrin and Förster. *Biophotonics Int* **11**(9):42–45.

De Angelis DA. 1999. Why FRET over genomics?. *Physiol Genomics* **1**:93–99.

Lilley DMJ, Wilson TJ. 2000. Fluorescence resonance energy transfer as a structural tool for nucleic acids. *Curr Opin Chem Biol* **4**:507–517.

Selvin PR. 1995. Fluorescence resonance energy transfer. *Methods Enzymol* **246**:300–334.

Wemmer DA, Case DA, Millar DP, eds. 2002. Biopolymers nucleic acid sciences, fluorescence spectroscopy and nucleic acids. *Biopolymers* **61**(3):143–242.

Wieb Van Der Meer B, Coker G, Simon Chen SY. 1991. *Resonance energy transfer theory and data*. Wiley-VCH, New York.

Theory—Multiple Acceptors

Jones GM, Wofsy C, Aurell C, Sklar LA. 1999. Analysis of vertical fluorescence resonance energy transfer from the surface of a small-diameter sphere. *Biophys J* **76**:517–527.

Rolinski OJ, Birch DJS. 2002. Structural sensing using fluorescence nanotomography. *J Chem Phys* **116**(23):10411–10418.

Uhlik F, Limpouchova Z, Matejicek P, Prochazka K, Tuzar Z, Webber S. 2002. Nonradiative excitation energy transfer in hydrophobically modified amphiphilic block copolymer micelles: theoretical model and Monte Carlo simulations. *Macromolecules* **35**:9497–9505.

PROBLEMS

P13.1. *Calculation of a Distance from the Transfer Efficiency*: Use the emission spectra in Figure 13.35 to calculate the distance from the indole donor to the dansyl acceptor. Assume that there is a single D–A distance, and that diffusion does not occur during the donor excited-state lifetime. The Förster distance $R_0 = 25.9$ Å, and the donor-alone lifetime is 6.8 ns. What is the D–A distance? What is the donor lifetime in the TUD D–A pair?

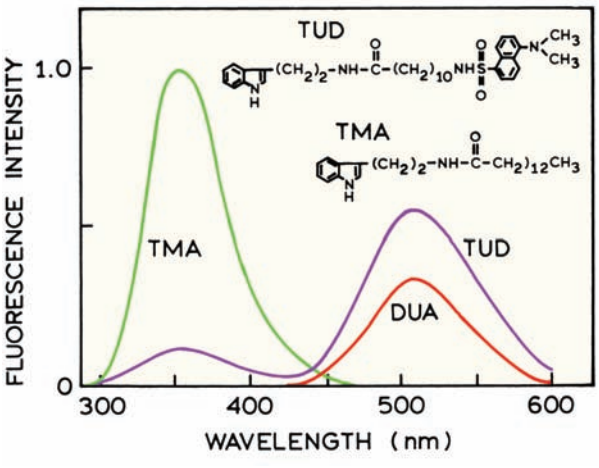

Figure 13.35. Emission spectra of a donor control (TMA) and a donor–acceptor pair (TUD) in propylene glycol at 20°C. DUA is an acceptor-only analogue. Revised from [98].

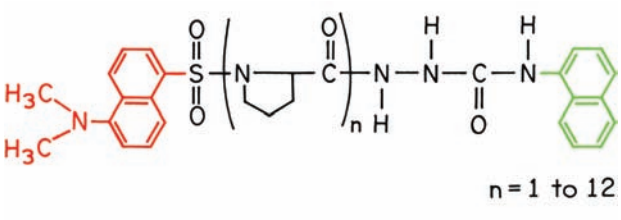

Figure 13.36. Structure of dansyl-(L-prolyl)$_n$-α-naphthyl used for determining the effects of distance on energy transfer. Revised from [18].

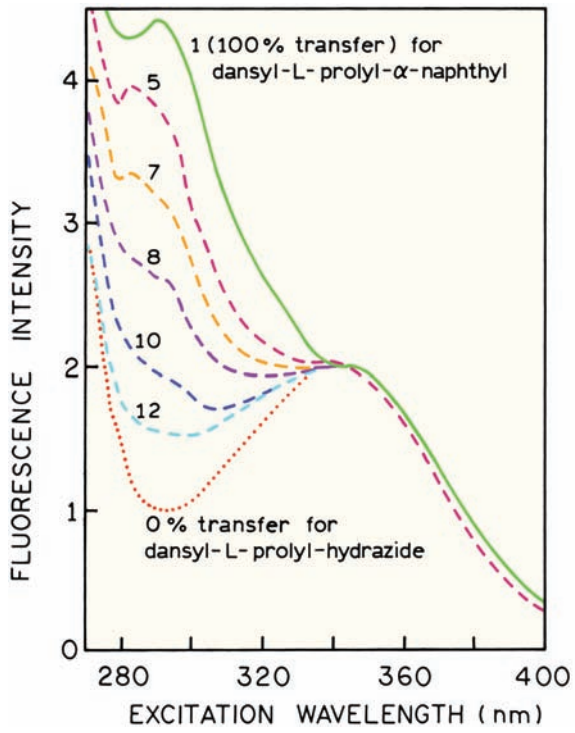

Figure 13.37. Excitation spectra of dansyl-(L-prolyl)$_n$-α-naphthyl molecules. Spectra are shown for dansyl-L-prolyl-hydrazide (dotted), dansyl-L-prolyl-α-naphthyl (solid), and dansyl-(L-prolyl)$_n$-α-naphthyl (dashed); n = 5, 7, 8, 10, and 12. Emission was detected at the dansyl emission maximum near 450 nm. Revised from [18].

P13.2. *Measurement of FRET efficiencies (E) from fluorescence intensities and lifetimes*: Use eq. 13.11 to derive the expressions for E based on intensities (eq. 13.13) or lifetimes (13.14).

P13.3. *Distance Dependence of Energy Transfer*: The theory of Förster states that the rate of energy transfer depends on $1/r^6$, where r is the donor-to-acceptor distance. This prediction was tested experimentally using naphthyl donors and dansyl acceptors linked by rigid polyprolyl spacers (Figure 13.36). Figure 13.37 shows the excitation spectra for this series of D–A pairs. Assume that each prolyl spacer contributes 2.83 Å to the spacing, and that the distance ranges from 12 (n = 1) to 43 Å (n = 12).

Use the excitation spectra to demonstrate that k_T depends on $1/r^6$. Note that the dansyl acceptor absorbs maximally at 340 nm and the naphthyl donor has an absorption maximum at 290 nm. Excitation spectra were recorded with the emission monochromator centered on the dansyl emission near 450 nm. What is R_0 for this D–A pair?

P13.4. *Effect of Spectral Overlap on the Rate of Energy Transfer*: Haugland et al.[20] investigated the effect of the magnitude of the spectral overlap integral on the rate of fluorescence energy transfer. For this study they used the steroids shown in Figure 13.38. They measured the fluorescence lifetimes of compounds I and II. The indole moiety is the donor that transfers energy to the ketone acceptor. Both the absorption spectrum of the ketone and the emission spectrum of the indole are solvent sensitive. Specifical-

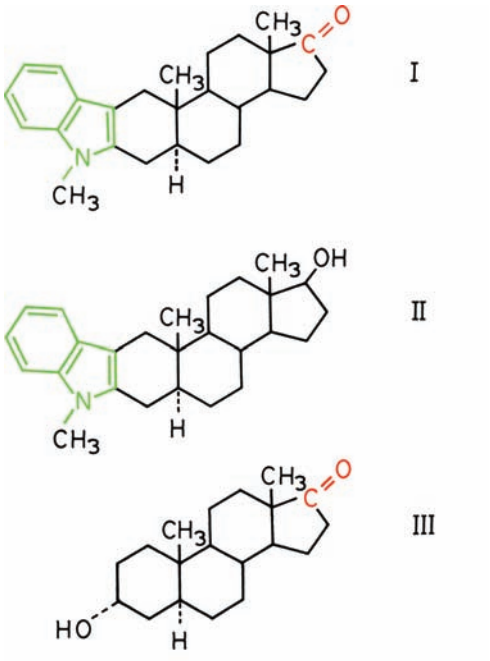

Figure 13.38. Structure of the rigid steroid donor–acceptor pair (I), the steroid containing the donor alone (II), and the steroid containing the acceptor alone (III). Indole is the donor and the carbonyl group is the acceptor. Revised from [20].

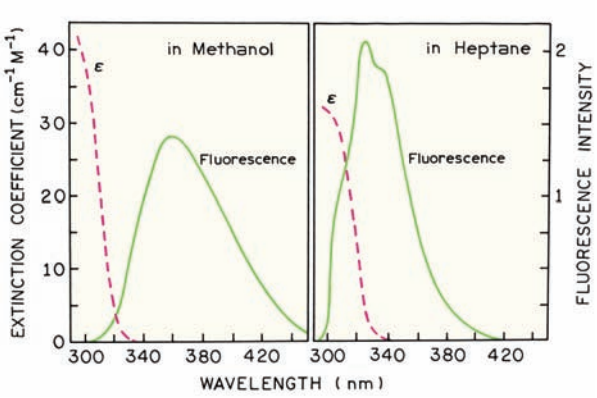

Figure 13.39. Overlap of emission spectrum of the indole donor (II) with the absorption spectrum of the carbonyl acceptor (III). Revised from [20].

ly, the emission spectrum of indole shifts to shorter wavelengths and the absorption spectrum of the ketone shifts to longer wavelengths as the solvent polarity decreases (Figure 13.39). These shifts result in increasing spectral overlap with decreasing solvent polarity.

Use the data in Table 13.5 to demonstrate that k_T is proportional to the first power of the extent of spectral overlap (J).

P13.5. *Calculation of a Förster Distance*: Calculate the Förster distance for the tryptophan-to-dansyl donor–acceptor pair shown in Figure 13.8. The quantum yield of the donor is 0.21.

P13.6. *Optical Assay for cAMP*: Figure 13.40 shows the emission spectra of a protein kinase that changes conformation in the presence of cAMP, and dissociates completely in the presence of a protein kinase inhibitor (PKI). The catalytic subunit is labeled with fluorescein (Fl-C) and the regulatory subunit is labeled with rhodamine (Rh–R). Derive an expression relating the ratio of donor to acceptor intensities to the protein kinase–cAMP dissociation constant. Assume that the donor and acceptor quantum yields are unchanged upon binding cAMP, except for the change in energy transfer. Describe how the conformational change, and change in RET, can be used to measure the concentration of cAMP.

Table 13.5. Fluorescence Spectral Properties of I and II in a Series of Solvents[a]

Solvent	τ (ns) I	τ (ns) II	J (cm⁶/m mole x 10^{19})
Methanol	5.3	5.6	1.5
Ethanol	5.6	6.5	3.0
Dioxane	3.6	5.4	13.0
Ethyl acetate	3.3	4.7	12.8
Ethyl ether	2.1	4.5	30.0
Heptane	1.1	2.8	60.3

[a]From [20].

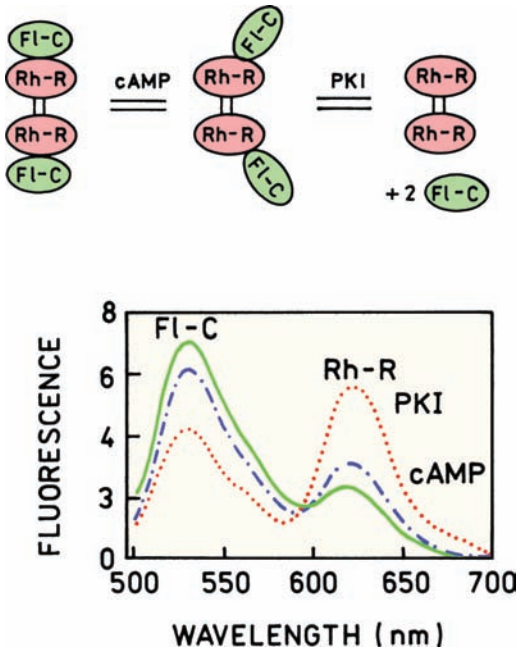

Figure 13.40. Emission spectra and schematic for the effect of cAMP and PKI on the emission spectra of the $(Rh\text{-}R)_2$–$(Fl\text{-}C)_2$ complex. Revised and reprinted with permission from [99]. Copyright © 1993, American Chemical Society.

P13.7. *Characteristics of a Closely Spaced D–A Pair*: Assume you have isolated a protein that contains a single-tryptophan residue, and binds dinitrophenol (DNP) in the active site. The absorption spectrum of DNP overlaps with the emission spectrum of the tryptophan residue. Assume R_0 = 50 Å and that DNP is not fluorescent. The fluorescence intensities of the tryptophan residue are 20.5 and 4.1 in the absence and presence of DNP, respectively, after correction for the inner filter effects due to the DNP absorption.

a. What is the transfer efficiency

b. Assume that the unquenched lifetime is 5 ns. What is the expected lifetime in the presence of DNP?

c. What is the transfer rate?

d. What is the distance between the tryptophan and the DNP?

e. Assume that the solution conditions change so that the distance between the tryptophan and the DNP is 20 Å. What is the expected intensity for the tryptophan fluorescence?

f. For this same solution (r = 20 Å) what would be the effect on the fluorescence intensity of a 1% impurity of a second protein that did not bind DNP? Assume this second protein has the same lifetime and quantum yield.

g. What lifetime would you expect for the sample that contains the impurity? Would this lifetime provide any indication of the presence of an impurity?

P13.8. *Effect of* κ^2 *on the Range of Possible Distances*: Suppose you have a donor- and acceptor-labeled protein that displays the following steady-state anisotropies.

Fluorophore	τ (ns)	r_D or r_A	r_0
Donor-alone control	5 ns	0.1	0.4
Acceptor	15 ns	0.05	0.4

Using an assumed value of $\tau^2 = 2/3$, the D–A distance was calculated to be 25 Å, and R_0 is also equal to 25 Å. Assume the protein displays a rotational correlation time of 5 ns. Use the data provided to calculate the range of distances possible for the D–A pair.

P13.9. *Effect of Acceptor Underlabeling on the Calculated Transfer Efficiency*: Suppose you have a presumed D–A pair. In the absence of acceptor the donor displays a steady-state intensity F_D = 1.0, and in the presence of acceptor F_{DA} = 0.5. Calculate the transfer efficiency assuming the fractional labeling with acceptor (f_A) is 1.0 or 0.5. How does the change in f_A affect the calculated distance?

P13.10. *FRET Efficiency from the Acceptor Intensities*: Derive eq. 13.25 for the case in which donor labeling is complete; f_D = 1.0. Also derive eq. 13.25 for the case when donor labeling is incomplete (f_D < 1).

P13.11. *Correction for Overlapping Donor and Acceptor Emission Spectra*: Equation 13.25 does not consider the possible contribution of the donor emission at the wavelength used to measure acceptor fluorescence (λ_A). Derive an expression for the enhanced acceptor fluorescence when the donor emits at λ_A. Explain how the apparent transfer efficiency, calculated without consideration of the donor contribution, would be related to the true transfer efficiency.

P13.12. Suppose that you have a protein with a single-tryptophan residue. Assume also that the protein noncovalently binds a ligand that serves as an RET acceptor for the tryptophan residue, and that the acceptor site is allosterically linked to the donor site such that acceptor binding induces an additional rate of donor quenching k_q in addition to k_T.

What is the apparent transfer efficiency upon acceptor binding in terms of τ_D, k_T, and k_q? Is the apparent value (E_D) smaller or larger than the true value (E)?